Proximity effect of time-reversal symmetry broken noncentrosymmetric superconductors

Tim Kokkeler,[1,2,*] Alexander Golubov,[2] Sebastian Bergeret,[3,1] and Yukio Tanaka[4,5]
[1]*Donostia International Physics Center (DIPC), 20018 Donostia–San Sebastián, Spain*
[2]*University of Twente, 7522 NB Enschede, The Netherlands*
[3]*Centro de Física de Materiales (CFM-MPC), Centro Mixto CSIC-UPV/EHU, 20018 Donostia–San Sebastián, Spain*
[4]*Department of Applied Physics, Nagoya University, 464-8603 Nagoya, Japan*
[5]*Research Center for Crystalline Materials Engineering, Nagoya University, 464-8603 Nagoya, Japan*

(Received 6 June 2023; revised 21 July 2023; accepted 28 July 2023; published 5 September 2023)

In noncentrosymmetric superconductors the pair potential has both even-parity singlet and odd-parity triplet components. If time-reversal symmetry is broken, the superconducting phase of these components is not the same, for example in anapole superconductors. In this paper it is shown that breaking time-reversal symmetry by a phase difference between the two components significantly alters both the density of states and the conductance in $s+$helical p-wave superconductors. The density of states and conductance in $s+$chiral p-wave superconductors are less influenced by adding a phase difference because time-reversal symmetry is already broken in the $s+p$-wave superconductor. The Tanaka-Nazarov boundary conditions are extended to 3D superconductors, allowing us to investigate a greater variety of superconductors, such as Balian-Werthamer superconductors, in which the direction of the d vector is parallel to the direction of momentum. The results are important for the determination of pair potentials in potentially time-reversal symmetry broken noncentrosymmetric superconductors.

DOI: 10.1103/PhysRevB.108.094503

I. INTRODUCTION

Ever since the discovery of high-temperature superconductors, much attention has been paid to unconventional superconductors [1–5], with for example triplet [1,6–23] or odd-frequency [8,24–35] pairing. Historically, most attention has been paid to superconductors in which time-reversal symmetry and inversion symmetry are not broken. In such superconductors the pair potential is either even parity or odd parity. However, if inversion symmetry is broken, for example in materials whose crystal structure breaks inversion symmetry, a type of superconductivity can emerge that is neither even parity nor odd parity [12,36–46]. In certain materials even the mixing parameter, the ratio between the singlet and triplet components, can be varied using electron irradiation [47].

Moreover, there exist several unconventional superconductors, including possibly Sr_2RuO_4, in which time-reversal symmetry is broken [1,14,48–74]. For example, in chiral superconductors [7], time-reversal symmetry is broken in the bulk. Next to this, time-reversal symmetry has been predicted to be spontaneously broken near the surface of d-wave superconductors [75–83].

In recent advances attention has been paid to so-called anapole superconductors. In anapole superconductors there exists a nonzero phase difference between the singlet and the triplet components [84–88]. Candidates for anapole superconductivity are UTe_2 [84–86] or narrow-gap semiconductors, for example $Cu_xBi_2Se_3$ or $Sn_{1-x}In_xTe$ [87]. In such superconductors, both time-reversal symmetry (T) and inversion symmetry (P) are broken while the product of time-reversal and inversion symmetry (PT) is preserved. They provide an analogy to axion electrodynamics [89,90], and may be used for future applications. For example, anapole superconductors may be suitable for nonreciprocal transport in Josephson junctions, such as the Josephson diode effect, since the requirements of time-reversal and inversion symmetry breaking are already met by the intrinsic properties of the superconductor. This greatly simplifies the geometry of the junctions needed for such effects. Next to this, heavy-fermion noncentrosymmetric superconductors, such as $CePt_3Si$ [12], UIr [38], $CeRh_2As_2$ [91], and $CeCu_2Si_2$ [92], also have magnetic ordered phases, which opens up the possibility of a P and T broken phase in those superconductors as well. However, so far little is known about the proximity effect induced by and the transport properties of anapole superconductors.

The simplest model for a superconductor which breaks both time-reversal symmetry and inversion symmetry is an $(i)s+p$-wave superconductor, in which there exists a nonzero phase difference between the singlet and the triplet correlations. Indeed, the phase difference provides the time-reversal symmetry breaking, while the presence of both even-parity s-wave and odd-parity p-wave amplitudes indicates inversion symmetry is broken. In fact, if the phase difference is an odd multiple of $\pi/2$ such superconductors do obey PT symmetry, and are therefore the simplest model of anapole superconductors.

The proximity effect and transport properties of noncentrosymmetric or time-reversal symmetry broken superconductors have been studied in detail in several limits, showing that they strongly depend on the presence of both singlet and triplet components and their relative strengths [93–105]. Recently a theory has been developed to calculate the

*tim.kokkeler@dipc.org

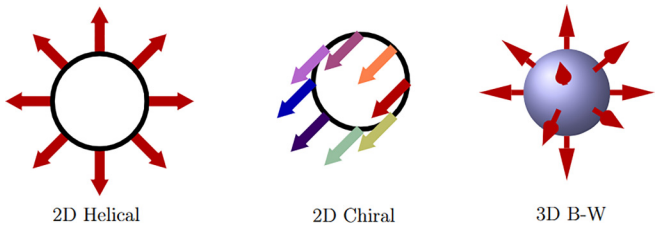

FIG. 1. The three different types of p-wave pair potentials used in this paper. The d vector is defined by its direction $\hat{\boldsymbol{d}}$ and its phase ψ, which is illustrated using color. For both the 2D helical and the 3D B-W superconductor phase the d vector is real, ψ is constant, but the direction of the d vector is momentum dependent. On the other hand, for the 2D chiral superconductor the phase depends on momentum, while the direction of the d vector is constant over the Fermi surface. In each case the magnitude of the gap is isotropic.

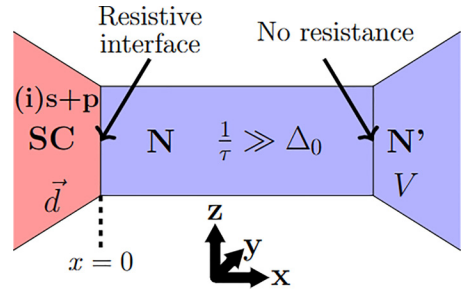

FIG. 2. The setup used in our calculations. The junction consists of a dirty ($1/\tau \gg \Delta_0$) normal-metal bar sandwiched between a superconducting electrode and a normal metal. The superconductor has both singlet s-wave correlations and triplet p-wave correlations characterized by the d vector $\boldsymbol{d}$. A voltage V is applied to the normal metal, while the superconducting electrode is grounded. The interface with the normal-metal electrode has no boundary resistance ($\gamma_{\rm BS} = 0$). The interface with the superconductor is resistive, and Tanaka-Nazarov boundary conditions are used.

proximity effect of noncentrosymmetric superconductors in dirty normal metals using the Keldysh-Usadel formalism [106–108]. Those works focus on time-reversal symmetric $s+$helical p-wave superconductors and on $s+$chiral superconductors in which there is no phase difference between the singlet and triplet components for the mode of normal incidence.

In this work, we use the mentioned theory to explore the density of states, pair amplitudes, and conductance in the presence of an arbitrary phase difference between the s-wave and p-wave components of the pair potential in the superconductor. We will refer to such superconductors as $(i)s+p$-wave superconductors. We calculate the conductance in SNN junctions with $(i)s+p$-wave superconductors. We show that the phase difference has a large influence on the proximity effect induced by $(i)s+$helical p-wave superconductors, and show that in the absence of time-reversal symmetry the density of states, pair amplitudes, and conductance are significantly altered. Notably, the quantization of the zero-energy density of states and the zero-bias conductance in $s+$helical p junctions disappears in the presence of a phase difference between the singlet and triplet components. Next to this, we show that for $(i)s+$chiral p-wave superconductors, for which time-reversal symmetry is broken by the p-wave component of the pair potential even in the absence of an s-wave component, the phase difference between the singlet and triplet correlations has a much smaller influence on the proximity effect. Our results highlight the importance of confirming the presence or absence of time-reversal symmetry in noncentrosymmetric superconductors.

Since the proposed anapole superconductors are three-dimensional [84], we extend the Tanaka-Nazarov boundary condition to 3D unconventional superconductors and study the Balian-Werthamer (B-W) phase that was first found in helium [109–111]. The B-W phase is the natural three-dimensional generalization of the 2D helical p-wave phase, the d vector is real and parallel to the direction of momentum, and the magnitude of the gap is isotropic as illustrated in Fig. 1. We show that contrary to junctions with 2D p-wave superconductors, junctions with 3D p-wave superconductors may have a zero-bias conductance dip instead of peak in short diffusive junctions. For long junctions, there exists a sharp peak with a width of the order of the Thouless energy due to coherent Andreev reflection. With this, we provide a systematic study of p and T symmetry broken superconductors in different dimensions.

II. THEORY

We consider the SNN junction shown in Fig. 2, consisting of a dirty normal-metal bar, with a scattering rate $1/\tau$ much larger than any other relevant energy scale except the Fermi energy, sandwiched between a normal-metal electrode to which a voltage may be applied, and an $(i)s+p$-wave superconductor with arbitrary phase difference between the singlet and triplet components:

$$\hat{\Delta}(\phi) = \Delta_0 \left(e^{i\frac{\pi}{2}\chi_t} \frac{1}{\sqrt{r^2+1}} + \frac{r}{\sqrt{r^2+1}} \boldsymbol{d}(\phi)\cdot\boldsymbol{\sigma} \right), \qquad (1)$$

where Δ_0 is a real scalar, $\boldsymbol{d}(\phi)$ is the d vector, an angle-dependent vector that is conventionally used to describe the spin dependence of the pair potential, ϕ is the angle between the direction of momentum and the normal to the S/N surface in Fig. 2, $\boldsymbol{\sigma}$ is the vector of Pauli matrices in spin space, r is the mixing parameter between the even-parity singlet s-wave component and the odd-parity triplet p-wave component of the pair potential, and χ_t is the phase difference between the singlet and triplet components. The singlet component of the pair potential will be referred to as Δ_s, the triplet as Δ_p. For $r = 0$ the expression reduces to conventional s-wave superconductivity; as $r \to \infty$ a p-wave superconductor is obtained. The d vector is different for different types of p-wave superconductivity. Because p-wave superconductors are odd parity, it necessarily satisfies $\boldsymbol{d}(\phi+\pi) = -\boldsymbol{d}(\phi)$.

Using the basis $(\psi_{\uparrow,k}, \psi_{\downarrow,k}, \psi^\dagger_{\downarrow,-k}, -\psi^\dagger_{\uparrow,-k})$, the Bogoliubov–de Gennes (BdG) Hamiltonian is

$$H(k) = \xi\tau_3 + \hat{\Delta}(\phi)\tau_2, \qquad (2)$$

where ξ is the single-particle energy and τ_i are the Pauli matrices in Nambu space. In this basis the time-reversal operator is $\mathcal{T} = \sigma_y\tau_3\mathcal{K}$, where $\mathcal{K}$ denotes complex conjugation.

Applying this to the BdG Hamiltonian, the condition for time-reversal symmetry, $H(-k) = \sigma_y\tau_3 H^*(k)\sigma_y\tau_3$, is satisfied if $\hat{\Delta}(\phi+\pi) = \sigma_y\hat{\Delta}^*\sigma_y$. For the set of pair potentials described by Eq. (1), the superconductor obeys time-reversal symmetry if χ_t is an even integer. Indeed, the time-reversal operation reverses the phase of all components and hence the phase difference between the singlet and triplet components. This phase difference remains the same only if it is a multiple of π; time-reversal symmetry is broken if this is not the case.

We assume that the Fermi energy is much larger than the other scales in the problem. In this case the Green's function is strongly peaked around the Fermi momentum, so that the quasiclassical formalism can be used. In the quasiclassical formalism the magnitude of momentum is fixed at the Fermi level; the resulting Green's function only depends on direction of momentum [112,113]. We consider the density of states and pair amplitude in the normal-metal bar at the interface with the superconducting electrode, and the conductance through the junction when applying a voltage to the normal metal; see Fig. 2. In many junctions thin films are used, in which the scattering length is limited by the thickness [114,115]. Therefore they can usually not be described by ballistic transport. Therefore, we assume that the normal-metal bar is in the dirty limit; that is, the scattering rate is high and the Green's function is almost isotropic. This allows us to use the Usadel equation to describe the N [112,113]. Notably, the superconductor itself is assumed to be clean, so that unconventional superconductivity is allowed. Next to this, we assume that the bar is either very wide or very narrow compared to the thermal diffusion length in the directions perpendicular to the transport direction, so that an effectively one-dimensional model may be used:

$$D\partial_x(\check{G}\partial_x\check{G}) = [iE\tau_3, \check{G}], \tag{3}$$

where D is the diffusion constant of the normal-metal bar, $\check{G}$ is the isotropic component of the Green's function in Keldysh-Nambu-spin space, and E is energy. The contact between the bar and the normal-metal electrode at $x = L$ is assumed to be very good, $\gamma_{BN} = 0$, so that the Green's function is continuous at this interface:

$$\check{G}(x = L) = \check{G}_N, \tag{4}$$

where $\check{G}_N$ is Green's function in the normal-metal electrode. It is equal to the Green's function in the bulk of a normal metal, with the retarded part given by $\check{G}^R_N = \tau_3$, and distribution functions $f_{L,T} = \frac{1}{2}(\tanh\frac{E+eV}{2kT} \pm \tanh\frac{E-eV}{2kT})$. At the interface with the superconductor ($x = 0$) we use the Tanaka-Nazarov boundary conditions [116,117], the extension of Nazarov's boundary conditions [118], derived using circuit theory, to junctions with unconventional superconductors:

$$\check{G}\nabla\check{G}(x = 0) = \frac{1}{\gamma_{\rm BS}L}\langle\check{S}(\phi)\rangle, \tag{5}$$

where [106]

$$\check{S}(\phi) = \tilde{T}\left(1 + T_1^2 + T_1(\check{C}\check{G} + \check{G}\check{C})\right)^{-1}(\check{C}\check{G} - \check{G}\check{C}), \tag{6}$$

$$\check{C} = \check{H}_+^{-1}(\check{\mathbb{1}} - \check{H}_-), \tag{7}$$

$$\check{H}_+ = \tfrac{1}{2}(\check{G}_{\rm S}(\phi) + \check{G}_{\rm S}(\pi - \phi)), \tag{8}$$

$$\check{H}_- = \tfrac{1}{2}(\check{G}_{\rm S}(\phi) - \check{G}_{\rm S}(\pi - \phi)). \tag{9}$$

Here $\check{G}_{\rm S}(\phi)$ is the bulk Green's function of an $(i)s + p$-wave superconductor. For the superconductors studied in this paper, the magnitude of $\boldsymbol{d}$ does not depend on momentum; hence $\boldsymbol{d}(\phi)$ can be written as $\hat{\boldsymbol{d}}(\phi)e^{i\psi(\phi)}$, where $\hat{\boldsymbol{d}}(\phi)$ is a unit vector and $\psi(\phi)$ is a phase. Specifically, for helical superconductors the d vector is real and hence $\psi(\phi) = 0$ with $\hat{\boldsymbol{d}}(\phi) = (\cos\phi, \sin\phi, 0)$, while for chiral superconductors $\psi(\phi) = \phi$ and $\hat{\boldsymbol{d}}(\phi) = (0, 0, 1)$. Therefore, using the basis $(\psi_\uparrow, \psi_\downarrow, \psi_\downarrow^\dagger, -\psi_\uparrow^\dagger)$, the bulk Green's function $\check{G}_{\rm S}(\phi)$ is given by [107]

$$\begin{aligned}\check{G}_{\rm S}(\phi) = {}& \frac{1}{2}[1 + \hat{\boldsymbol{d}}(\phi)\cdot\boldsymbol{\sigma}] \otimes \frac{1}{\sqrt{E^2 - |\Delta_+|^2}}\begin{bmatrix} E & \Delta_+ \\ -\Delta_+^* & -E\end{bmatrix} \\ & + \frac{1}{2}[1 - \hat{\boldsymbol{d}}(\phi)\cdot\boldsymbol{\sigma}] \otimes \frac{1}{\sqrt{E^2 - |\Delta_-|^2}}\begin{bmatrix} E & \Delta_- \\ -\Delta_-^* & -E\end{bmatrix}, \\ \Delta_\pm = {}& \frac{e^{i\frac{\pi}{2}\chi_t} \pm re^{i\psi(\phi)}}{\sqrt{r^2+1}}.\end{aligned} \tag{10}$$

The brackets $\langle\cdot\rangle$ indicate angular averaging over all modes that pass through the interface, the symbol $\otimes$ is used to denote a Kronecker product, $\gamma_{\rm BS} = R_{\rm B}/R_{\rm d}$ is the ratio between the boundary resistance and the normal-state resistance of the dirty normal-metal bar, $T_1 = \tilde{T}/(2 - \tilde{T} + 2\sqrt{1-\tilde{T}})$, and $\tilde{T}$ is the interface transparency given by [23]

$$\tilde{T}(\phi) = \frac{\cos^2\phi}{\cos^2\phi + z^2}, \tag{11}$$

where z is the Blonder-Tinkham-Klapwijk (BTK) parameter. We do not take into account the Fermi surface mismatch, assuming that the magnitude of the Fermi momentum is of similar magnitude in the superconductor and the normal metal.

The equations for the retarded part $\check{G}^R$ in Keldysh space are solved numerically. The advanced Green's function $\check{G}^A$ is directly related to the retarded part via $\check{G}^A = -\tau_3(\check{G}^R)^\dagger\tau_3$ [112,113]. Based on the solutions for the retarded and advanced components, the Keldysh component can be found numerically using the distribution function $\check{h} = \hat{f}_L \otimes \mathbf{1}_\tau + \hat{f}_T \otimes \tau_3$ for $\check{G}^K = \check{G}^R\check{h} - \check{h}\check{G}^A$ [112,113], where $\mathbf{1}_\tau$ is the identity matrix in Nambu space, τ_3 is the third Pauli matrix in Nambu space, and $\hat{f}_L$ and $\hat{f}_T$ are the so-called longitudinal and transverse components of the distribution function [119,120] to be determined.

We consider the density of states and pair amplitudes at the interface with the superconductor, given by

$$\rho = {\rm Tr}[(\mathbf{1}_\sigma \otimes \tau_3)\check{G}^R(x = 0)]/4, \tag{12}$$

$$F^R_{s1,2} = {\rm Tr}[(\mathbf{1}_\sigma \otimes \tau_{1,2})\check{G}^R(x = 0)]/4, \tag{13}$$

$$F^R_{t1,2} = {\rm Tr}[(\hat{\boldsymbol{d}}\cdot\boldsymbol{\sigma} \otimes \tau_{1,2})\check{G}^R(x = 0)]/4, \tag{14}$$

where $\tau_{1,2,3}$ are the Pauli matrices in Nambu space and $\sigma_{1,2,3}$ the Pauli matrices in spin space, while $\mathbf{1}_\sigma$ is the identity matrix in spin space.

The functions $F_{s1,2}$ and $F_{t1,2}$ are the pair amplitudes $\langle\psi_\uparrow\psi_\downarrow - \psi_\downarrow\psi_\uparrow\rangle$ and $\langle\psi_\uparrow\psi_\downarrow + \psi_\downarrow\psi_\uparrow\rangle$ in the normal metal,

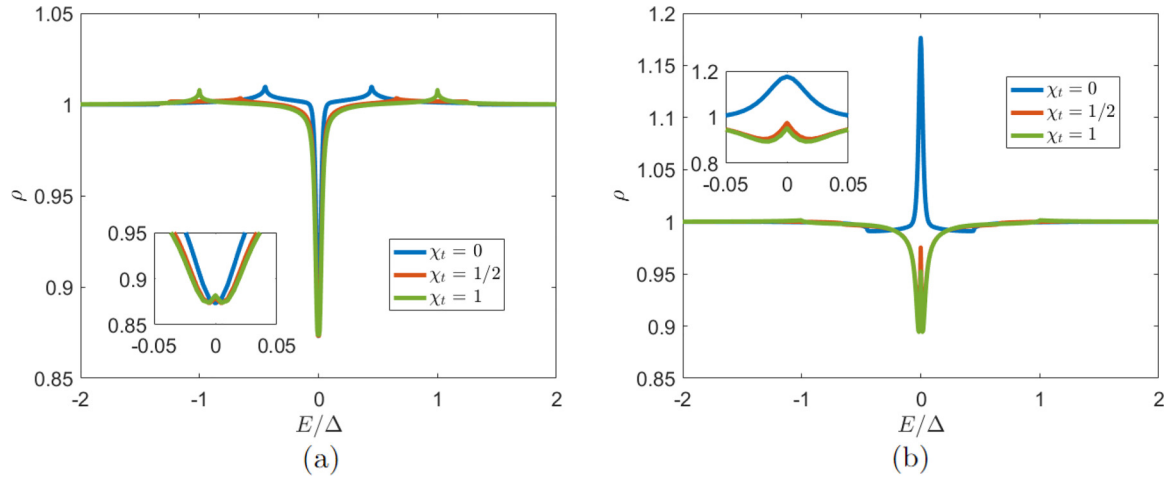

FIG. 3. The local density of states for $e^{i\chi_t \frac{\pi}{2}}$ $s+$ helical p-wave superconductors for s-wave-dominant, $r = 0.5$ (a) and p-wave-dominant, $r = 2$ (b) superconductors. If the s-wave component is dominant, for $\chi_t = 0$ at $E = 0$ only singlet correlations are present. For $\chi_t \neq 0$ also triplet correlations are present, enhancing the zero-energy density of states. If the p-wave component is dominant, for $\chi_t = 0$ there are only triplet correlations, for $\chi_t \neq 0$ also singlet pairs, suppressing the density of states. Other parameters are set to $\gamma_{\rm BS} = 2$, $z = 0.75$, $E_{\rm Th}/\Delta_0 = 0.02$.

where $\uparrow, \downarrow$ correspond to the ± 1 eigenstates of $\hat{\boldsymbol{d}} \cdot \boldsymbol{\sigma}$. In the absence of the superconductor these pair correlations are absent; however, due to the proximity effect they can be nonzero. Due to the Pauli principle, the singlet correlations are even-frequency correlations on the Matsubara axis, thus satisfying $F^R_{s1,2}(-E) = [F^R_{s1,2}(E)]^*$, while the triplet correlations are odd-frequency correlations, therefore satisfying $F^R_{t1,2}(-E) = -[F^R_{t1,2}(E)]^*$. The subscripts 1, 2 refer to the traces of the $\tau_{1,2}$ components, respectively, that is, to the phase of the superconductor. For an s-wave superconductor at zero phase only the component F_{s2} is nonzero; if its phase is $\pm\pi/2$ only the component F_{s1} is nonzero. For a p-wave component at zero phase the conversion of ETO (even frequency triplet odd parity) to OTE pairing implies only the component F_{t1} to be nonzero in the metal; if its phase is $\pi/2$ only the component F_{t2} is nonzero. Similarly, if the superconductor is an $s+p$-wave superconductor, only F_{s2} and F_{t1} correlations are induced in the normal metal. However, if there is a phase difference between the $s+p$-wave correlations, all components may be induced and their proportion can be energy dependent.

Using the Keldysh component the conductance can be calculated as

$$\sigma = \frac{\partial I}{\partial V},$$
$$I = \frac{\sigma_N}{16e}\int_{-\infty}^{\infty} dE \mathrm{Tr}\{(\mathbf{1}_\sigma \otimes \tau_3)(\check{G}\nabla\check{G})^K\}, \tag{15}$$

where σ_N is the normal-state conductance of the bar and $(\check{G}\nabla\check{G})^K$ is the Keldysh component of $\check{G}\nabla\check{G}$.

III. HELICAL p-WAVE SUPERCONDUCTORS

In this section, we present the result for $(i)s+$ helical p-wave superconductors. For helical p-wave superconductors the d vector is given by $\boldsymbol{d}(\phi) = (\cos\phi, \sin\phi, 0)$. For $\chi_t = 0$, there is no time-reversal symmetry breaking and this model reduces to the model studied in [106–108]. Another special case is $\chi_t = 1$. In that case the quantities

$$\Delta_\pm = \frac{e^{i\frac{\pi}{2}\chi_t} \pm r}{\sqrt{1+r^2}}\Delta_0 \tag{16}$$

both have magnitude Δ_0, irrespective of r or angle ϕ. This implies that the double-peak structure obtained for $\chi_t = 0$ is not to be expected for $\chi_t = 1$.

The dependence of $|\Delta_\pm|$ on χ_t, r, and ϕ is described by

$$|\Delta_\pm|^2 = \left(1 \pm \frac{2r\cos\frac{\pi}{2}\chi_t}{1+r^2}\right)\Delta_0^2. \tag{17}$$

In the next section, we discuss the dependence of the density of states, pair amplitudes, and conductance on χ_t for various ratios of the s-wave and p-wave components of the pair potential while setting the other parameters equal to the values used in [108] for the case $\chi_t = 0$, that is, $\gamma_{\rm BS} = 2$, $z = 0.75$, and $\Delta_0/E_{\rm Th} = 50$.

A. Density of states and pair amplitudes

From the retarded part of the Green's function G^R, the local density of states at the SN interface ($x = 0$) can be extracted. The local density of states is shown in Fig. 3. For s-wave-dominant superconductors, Fig. 3(a), the zero-energy density of states is almost independent of χ_t; the phase difference between the s-wave and p-wave components of the pair potential only influences the details of the density of states. Most notably, the most pronounced peak shifts from $E = \Delta_-$ to $E = \Delta_0$ with increasing χ_t. On the other hand, for p-wave-dominant superconductors the zero-energy density of states is influenced by χ_t, as shown in Fig. 3(b). For $\chi_t = 0$ there is a large zero-energy peak. If χ_t is nonzero the zero-energy peak is highly suppressed; there are both a broad dip and a sharp peak centered at zero energy. In contrast to junctions with $s+$ helical p-wave superconductors with $\chi_t = 0$ the zero-energy density of states is not guaranteed to be higher than the normal density of states.

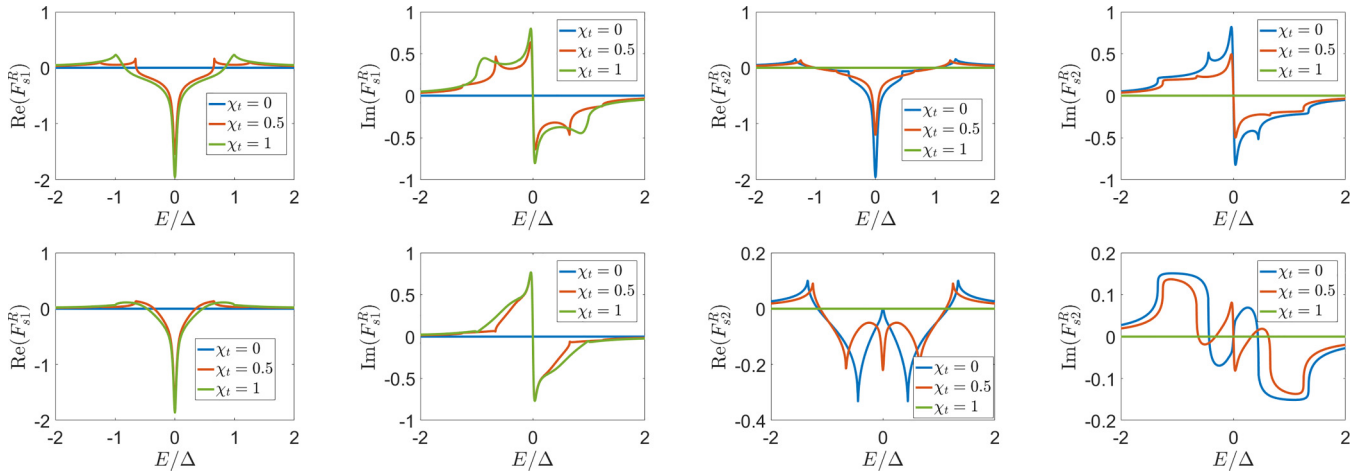

FIG. 4. The singlet pair amplitudes for $e^{i\chi_t \frac{\pi}{2}}$ $s+$helical p-wave superconductors for s-wave-dominant superconductors with $r = 0.5$ (top row) and p-wave-dominant superconductors with $r = 2$ (bottom row). The singlet pair amplitudes are even frequency and hence satisfy $F(-E) = F^*(E)$. Other parameters are set to $\gamma_{\mathrm{BS}} = 2$, $z = 0.75$, $E_{\mathrm{Th}}/\Delta_0 = 0.02$.

The singlet and triplet pair amplitudes are shown respectively in Figs. 4 and 5. The phase of the induced correlations depends on χ_t. For $\chi_t = 0$, that is, for $s+p$-wave superconductors, only F_{s2} and F_{t1} can be nonzero. On the other hand, for $\chi_t = 1$, that is, for $is+p$-wave superconductors, only F_{s1} and F_{t1} are nonzero. For $0 < \chi_t < 1$ all components of the pair amplitude can be nonzero and the phase of the correlations depends on energy.

For s-wave dominant superconductors, the real part of the singlet pair amplitudes, see Fig. 4 (top), is maximized at zero energy, regardless of χ_t. On the other hand, for the p-wave-dominant case, Fig. 4 (bottom), the singlet pair amplitudes vanish at zero energy if $\chi_t = 0$. In contrast, for nonzero χ_t the real parts of singlet pair amplitude are maximized at zero energy. Also here, the phase depends strongly on χ_t.

The triplet pair amplitudes depend more strongly on χ_t if the s-wave component of the pair potential is dominant. Indeed, for s-wave-dominant junctions with $\chi_t = 0$, Fig. 5 (top), the triplet pair amplitudes vanish at zero energy. On the other hand, for $\chi_t \neq 0$ the imaginary parts of the triplet pair amplitudes are maximized at zero energy. For p-wave-dominant superconductors, the imaginary parts of the triplet pair amplitude are maximized at zero energy for all χ_t, as shown in Fig. 5 (bottom). An increase of the phase difference between the singlet and triplet components suppresses this maximum, but only slightly. Summarizing, a nonzero χ_t enhances the subdominant pair amplitudes at zero energy, while only moderately altering the magnitude of dominant pair amplitudes. The phase χ_t does in all cases have a large influence on the phase of the induced correlations.

The different behavior of the local density of states and the pair amplitudes in the presence of a phase difference between singlet and triplet pair potentials can be explained using topology. The helical p-wave superconductor is a topological superconductor protected by time-reversal symmetry breaking [2,121,122]. The addition of an s-wave component

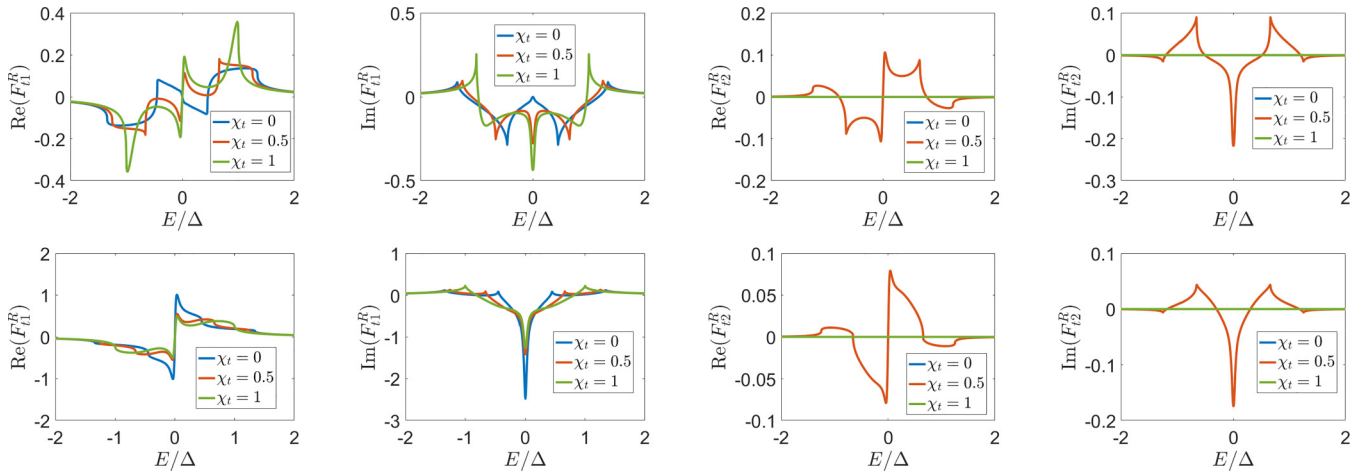

FIG. 5. The triplet pair amplitudes for $e^{i\chi_t \frac{\pi}{2}}$ $s+$helical p-wave superconductors for s-wave-dominant superconductors with $r = 0.5$ (top row) and p-wave-dominant superconductors with $r = 2$ (bottom row). The triplet pair amplitudes are odd frequency and hence satisfy $F(-E) = -F(E)^*$. For $\chi_t \in \{0, 1\}$ only τ_x components are induced because of the additional $\pi/2$ phase drop at the interface for triplet correlations. For $0 < \chi_t < 1$ the phase depends on energy. Other parameters are set to $\gamma_{\mathrm{BS}} = 2$, $z = 0.75$, $E_{\mathrm{Th}}/\Delta_0 = 0.02$.

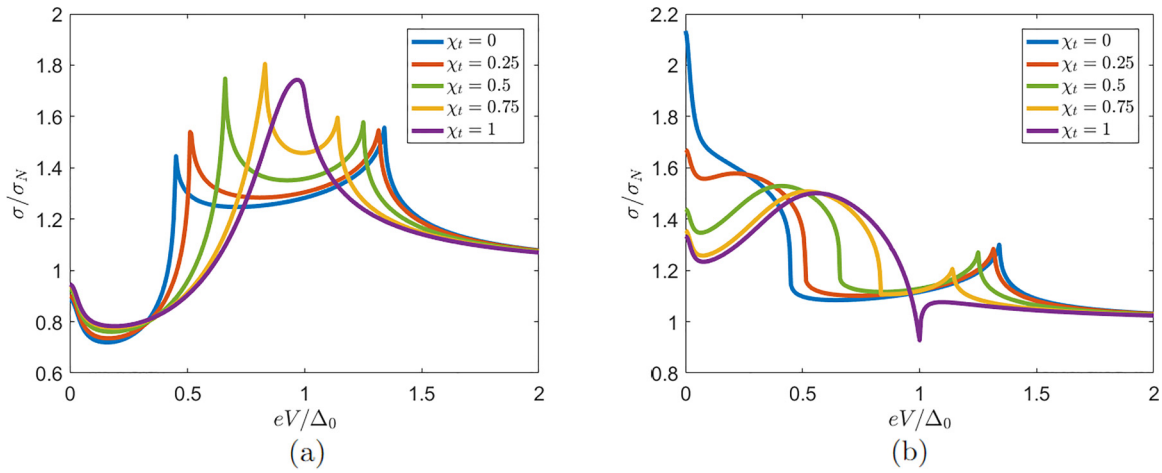

FIG. 6. The dependence of the conductance on the relative phase difference between the s-wave and helical p-wave components of the pair potential for $r = 0.5$ (left) and $r = 2$ (right). If there is no time-reversal symmetry breaking ($\chi_t = 0$), the conductance has sharp features at $|\Delta_\pm| = |\Delta_s \pm \Delta_p|$. As the phase difference between the s-wave and p-wave components of the pair potential increases, these features come together, resulting in one smooth peak for $\chi_t = 1$. Parameters are set to $\gamma_{\rm BS} = 2$, $z = 0.75$, $E_{\rm Th}/\Delta_0 = 0.02$.

does not violate the symmetries of the topological class, and zero-energy bound states appear also in the noncentrosymmetric case [123], and therefore a topological phase transition must appear when changing the mixing parameter from helical p wave to s wave. The gap closes if and only if $r = 1$, which must therefore be the topological phase boundary. On the other hand, for $is + p$-wave superconductors time-reversal symmetry is broken and there is no topological phase transition; all properties change continuously from s-wave to p-wave as the mixing parameter r is increased. For the zero-energy density of states and pair amplitudes, this can be shown explicitly. The density of states and pair amplitude at zero energy are fully determined by $\frac{\Delta_+}{|\Delta_+|}$ and $\frac{\Delta_-}{|\Delta_-|}$ [108,124]. If $\chi_t = 0$, both Δ_+ and Δ_- are necessarily real, and therefore, using that $\Delta_+ > 0$ by definition, the zero-energy density of states and pair potentials are fully determined by the sign of Δ_-. However, if $\chi_t \neq 0$ the quantities $\frac{\Delta_+}{|\Delta_+|}$ and $\frac{\Delta_-}{|\Delta_-|}$ are both complex and continuous functions of r. Therefore, at $E = 0$ the results are neither s wave nor p wave, but rather a mixture and both singlet and triplet correlations are present.

B. Conductance

The effect of a finite phase difference between the s-wave and the p-wave components of the pair potential on the conductance is illustrated in Fig. 6 for an s-wave-dominant superconductor with $r = 0.5$ [Fig. 6(a)] and a p-wave-dominant superconductor with $r = 2$ [Fig. 6(b)]. For $r = 0.5$ and $\chi_t = 0$ the conductance is maximized at $eV = \Delta_\pm$, but if $\chi_t = 1$ the peaks merge together into a single peak at Δ_0. Notably, a small peak at zero bias remains even for the time-reversal symmetry breaking superconductors. This is in contrast with the zero-bias conductance in junctions in which the time-reversal symmetry is broken by an exchange field, in which case the small peak disappears [108]. The difference can be explained as follows. Without an exchange field the correlations in the normal-metal bar decay on a length scale $\sqrt{D/(2E)}$, irrespective of the phase difference between the s-wave and p-wave components of the pair potential, which are not mixed. On the other hand, in the presence of an exchange field, the singlet and triplet components are mixed, and the correlations decay on a length scale $\sqrt{D/[2(E \pm h)]}$, where h is the exchange field strength. Therefore, in the presence of an exchange field, crossed Andreev reflection is suppressed, but in SNN junctions with time-reversal symmetry breaking superconductors it is preserved. The results for junctions in which the p-wave component of the pair potential is dominant, e.g., $r = 2$, are shown in Fig. 6(b). The sharp change in $d\sigma/dV$ at $eV = |\Delta_-|$ and the conductance peak at $eV = \Delta_+$ likewise get closer together, merging into a small conductance dip at $eV = \Delta_0$ for $\chi_t = 1$. Moreover, an increase of χ_t decreases the zero-bias conductance peak.

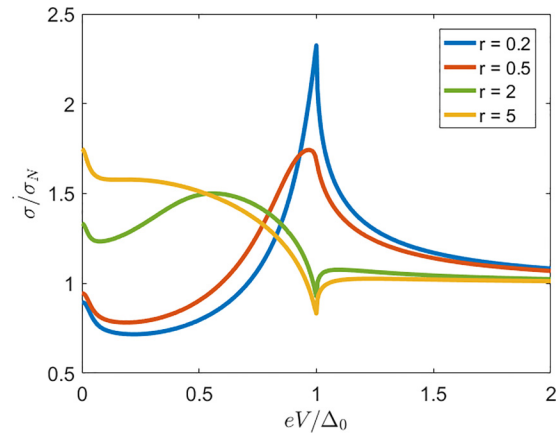

FIG. 7. The conductance of the junction for different mixing parameters r if $\chi_t = 1$. There is not a quantization of the zero-bias conductance peak, unlike for $\chi_t = 0$, but rather a continuous change between a small zero-bias conductance peak that does not exceed the normal-state conductance and has a width on the order of the Thouless energy for $r < 1$ and a larger peak for $r > 1$ that exceeds the normal-state conductance and may have a width larger than the Thouless energy. Other parameters are set to $\gamma_{\rm BS} = 2$, $z = 0.75$, $E_{\rm Th}/\Delta_0 = 0.02$.

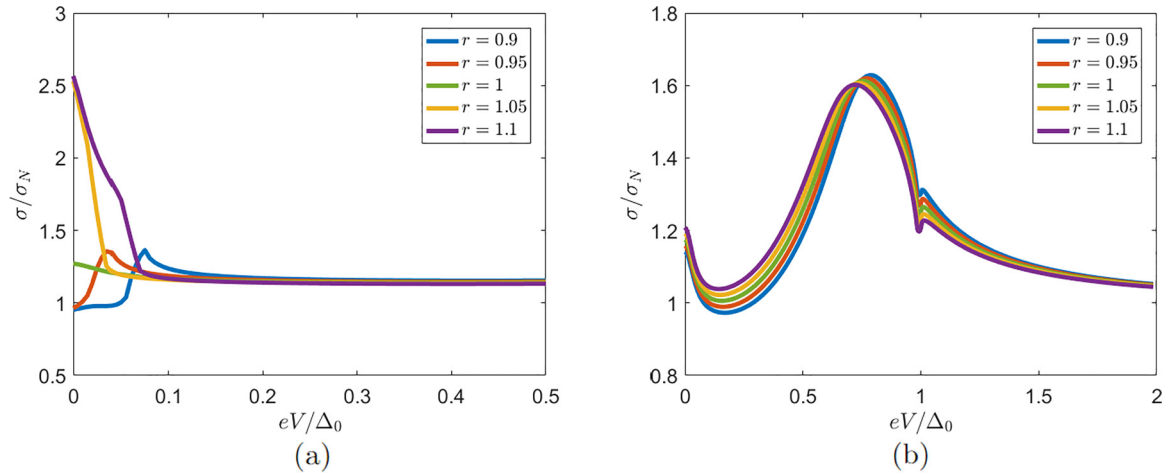

FIG. 8. The conductance near the transition between the s-wave-dominated and p-wave-dominated regime for $s+$ helical (a) and $is+$ helical (b) p-wave superconductors. For $s+$ helical p-wave superconductors there is a topological transition and the zero-bias conductance has a discontinuity at $r = 1$; for $is+$ helical p-wave superconductors the topological protection is broken and the zero-bias conductance is continuous at $r = 1$. Other parameters are set to $\gamma_{\rm BS} = 2$, $z = 0.75$, $E_{\rm Th}/\Delta_0 = 0.02$.

The dependence on the mixing parameter r is illustrated in Figs. 7 and 8. For an $is+p$-wave superconductor there is no quantization of the zero-bias conductance, as shown in Fig. 7. This can be understood as follows. The zero-bias conductance depends on the quantities $\Delta_\pm/|\Delta_\pm|$. As discussed before, for $\chi_t = 1$ these quantities are complex, with the phase depending on the actual value of r, and therefore, the zero-bias conductance depends nontrivially on r. This is in contrast with the case $\chi_t = 0$, when $\Delta_\pm/|\Delta_\pm|$ are both real, giving the quantization of conductance [108,124]. An analytical description can be found in the 1D case. The matrix $\check{C}(E=0,r)$ entering the boundary condition Eq. (7) is for $is+$ helical p-wave superconductors given by

$$\check{C}(E=0,r) = \begin{bmatrix} -ir\sigma_x & \sqrt{r^2+1}\mathbf{1}_\sigma \\ \sqrt{r^2+1}\mathbf{1}_\sigma & ir\sigma_x \end{bmatrix}, \tag{18}$$

where $\mathbf{1}_\sigma$ is the identity matrix in spin space and σ_x is the first Pauli matrix in spin space. For finite r the quantity $\check{C}(E=0,r)$ is finite, showing that there is no pole at $E=0$, in contrast to cases of a one-dimensional p-wave superconductor [106] or a two-dimensional $s+$ helical p-wave superconductor [107]. This means there is no zero-energy Andreev bound state for $is+p$-wave superconductors. The boundary quantity C changes continuously as a function of r, and in the limit $r\to\infty$ the p-wave expression is recovered; in the limit $r\to 0$ the s-wave expression is recovered, showing that the zero-bias conductance continuously changes from the value attained by s-wave superconductors to the value attained by p-wave superconductors.

The broadness of the peak can be understood by considering the poles of C, which is connected to the existence of the Andreev bound state in the clean limit [106]. The quantity C is for $is+p$-wave superconductors given by

$$\check{C}(\phi) = \check{H}_+^- - \check{H}_+^{-1}\check{H}_- = \frac{1}{E^2 - \left(\Delta_s^2 + \Delta_p^2\sin^2\phi\right)} \times \left(\sqrt{E^2-\Delta_0^2}\begin{bmatrix} E\mathbf{1}_\sigma & \Delta_{isp+}\mathbf{1}_\sigma \\ \Delta_{isp-}\mathbf{1}_\sigma & -E\mathbf{1}_\sigma \end{bmatrix} + \begin{bmatrix} \Delta_{isp+}\Delta_p\cos\phi\sigma_x & -E\Delta_p\cos\phi\sigma_x \\ -E\Delta_p\cos\phi\sigma_x & -\Delta_{isp+}\Delta_p\cos\phi\sigma_x \end{bmatrix}\right),$$

$$\Delta_{isp\pm} = i\Delta_s \pm \Delta_p\sin\phi\sigma_y. \tag{19}$$

The denominator has zeros for $E = \Delta_0\sqrt{\frac{1+r^2\sin^2\phi}{1+r^2}}$. Therefore, the conductance peak is enhanced for voltages satisfying $\Delta_s = \frac{\Delta_0}{\sqrt{r^2+1}} < eV < \Delta_0$. Thus, with increasing mixing parameter r the peak width increases, as confirmed by the results in Fig. 7.

The continuity of C as a function of r implies that the transition between the s-wave dominated as p-wave dominated regimes is vastly different for $s+$ helical and $is+$ helical p-wave superconductors, as shown in Fig. 8. For the $s+$ helical p-wave superconductors there is a topological phase transition at $r=1$ [125], which leads to a discontinuity of the conductance at zero bias [107], as shown in Fig. 8(a). On the other hand, for $is+$ helical p-wave superconductors the topological protection is absent and the conductance is continuous as a function of r, even at $r=1$; see Fig. 8(b). The conductance for $r\approx 1$ has similarities with both the conductance in s-wave junctions and the conductance in p-wave junctions. The zero-bias conductance for $r\approx 1$ is larger than the normal-state conductance, as for p-wave junctions. However, the peak at $eV=\Delta_0$ is distinctly larger than the one at $eV=0$, which is reminiscent of s-wave junctions.

IV. CHIRAL SUPERCONDUCTORS

The calculations were repeated for chiral superconductors. Chiral superconductors are distinctly different from helical superconductors; time-reversal symmetry is broken for the p-wave state, even in the absence of an s-wave component of the pair potential. In chiral superconductors, the phase of the p-wave correlations depends on the angle ϕ with the normal of the surface; the d vector is given by

$$\boldsymbol{d}(\phi) = e^{i\phi}(0,0,1). \tag{20}$$

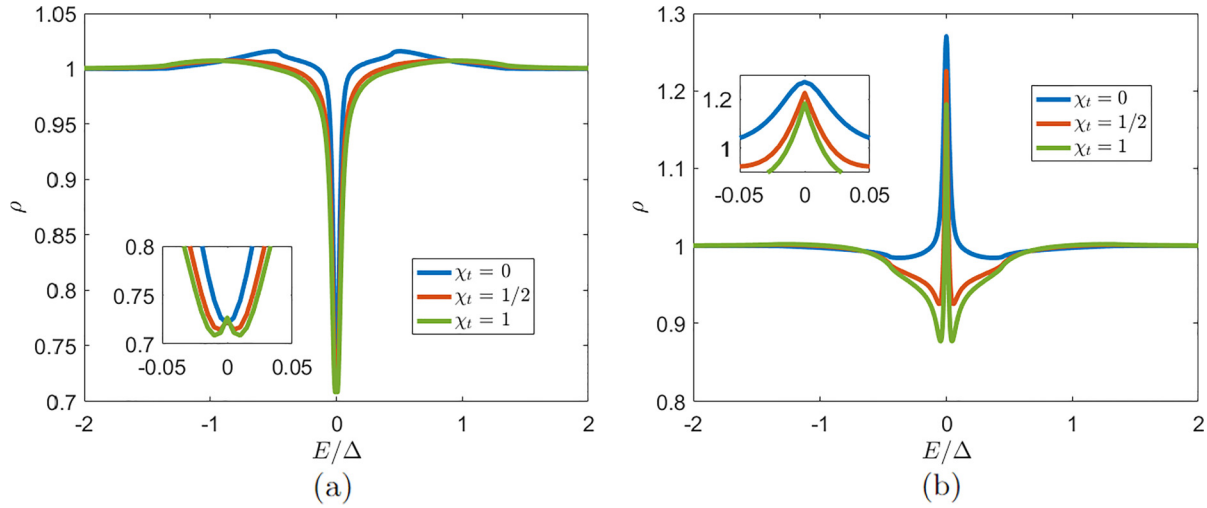

FIG. 9. The density of states in the $(i)s+$chiral p-wave superconductor junctions for different χ_t. If $r=0.5$ (a) there is a zero-energy dip; if $r=2$ (b) there is a zero-energy peak. For nonzero χ_t the dip and peak are suppressed because the nondominant pair amplitude is enhanced. Other parameters are set to $\gamma_{\rm BS}=2$, $z=0.75$, $E_{\rm Th}/\Delta_0=0.02$.

The phase difference between the s-wave and the p-wave pair amplitudes will be defined as the phase difference for the singlet and triplet correlations for the mode normal to the interface. For all calculations we used the same set of parameters as for the $(i)s+$helical p-wave superconductors, that is, $\gamma_{\rm BS}=2$, $z=0.75$, and $\Delta_0/E_{\rm Th}=50$.

For $(i)s+$chiral p-wave superconductors we define χ_t using the phase difference of the mode normal to the interface. The terms $s+$chiral p-wave or $is+$chiral p-wave superconductors will refer $\chi_t=0$ and $\chi_t=1$. In practice this means that a single material can act both as an $s+$chiral and an $is+$chiral superconductor, depending on in which direction the junction is made. For example in a setup with two disjointed SN junctions that make an angle of $\frac{\pi}{2}$ [108], both types can be probed.

A. Density of states and pair amplitudes

The local density of states for $s+$chiral p-wave junctions is shown in Fig. 9. The results are similar to those of $s+$helical p-wave junctions, although the effects of χ_t are smaller for $(i)s+$chiral p-wave junctions. If the s-wave component of the pair potential is dominant the zero-energy density of states is well below the normal density states, as shown in Fig. 9(a). If the p-wave component of the pair potential is dominant, see Fig. 9(b), the structure with both a broad dip and a narrow peak appears when χ_t is nonzero. It differs from the $s+$helical p-wave case by having a distinctly broader dip and a zero-energy density of states that is well above the normal density of states.

The pair amplitudes are shown in Figs. 10 and 11. The magnitudes of the dominant pair amplitude [Figs. 10 (top)

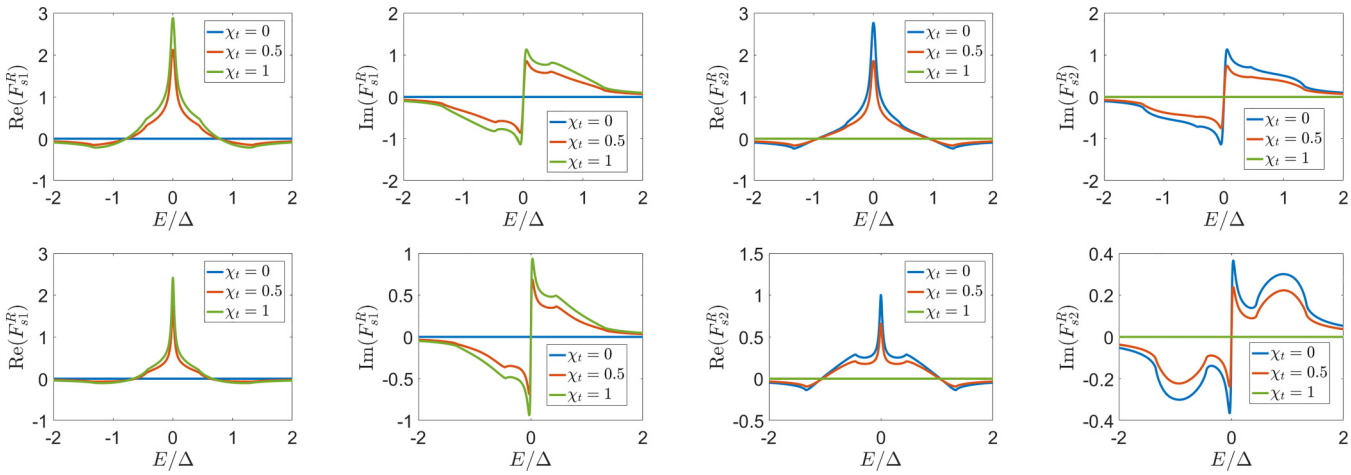

FIG. 10. The singlet pair amplitudes for $e^{i\chi_t\frac{\pi}{2}}$ $s+$chiral p-wave superconductors for s-wave-dominant superconductors with $r=0.5$ (top row) and p-wave-dominant superconductors with $r=2$ (bottom row). The singlet pair amplitudes are even frequency and hence satisfy $F(-E)=F^*(E)$. Other parameters are set to $\gamma_{\rm BS}=2$, $z=0.75$, $E_{\rm Th}/\Delta_0=0.02$.

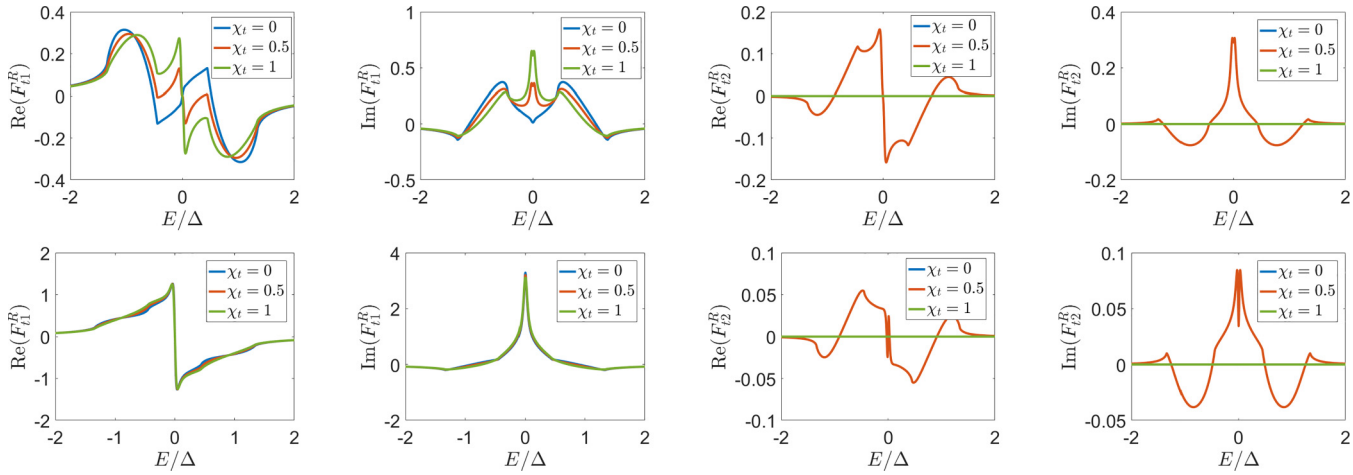

FIG. 11. The triplet pair amplitudes for $e^{i\chi_t \frac{\pi}{2}}$ $s+$chiral p-wave superconductors for s-wave-dominant superconductors with $r = 0.5$ (top row) and p-wave-dominant superconductors with $r = 2$ (bottom row). The triplet pair amplitudes are even frequency and hence satisfy $F(-E) = -F^*(E)$. Other parameters are set to $\gamma_{\mathrm{BS}} = 2$, $z = 0.75$, $E_{\mathrm{Th}}/\Delta_0 = 0.02$.

and 11 (bottom)] are, similarly to the $(i)s+$helical case, very similar for different χ_t, though the phase of the induced correlations strongly depends on χ_t. On the other hand, the results for the subdominant pair amplitude depend strongly on χ_t and they are distinctly different from the $s+$helical p-wave superconductors. First of all, even if $\chi_t = 0$ the subdominant component need not vanish at zero energy. Indeed, $\mathrm{Re}[F_{s2}(E=0)] \neq 0$ for triplet dominant pair potentials, see Figs. 10 (bottom), and similarly $\mathrm{Im}[F_{t1,2}(E=0)] \neq 0$ for singlet dominant junctions, as shown in Fig. 11 (top). This is due to the time-reversal symmetry breaking of the chiral p-wave component of the pair potential. Next to this, even for $\chi_t = 1$ there is a small and narrow dip around zero energy in the triplet pair amplitude. The singlet pair amplitude has a zero energy peak even for triplet dominant $s+$chiral p-wave superconductors. This peak increases when χ_t is increased.

These effects can be attributed to the angle dependence of the phase difference between the s-wave and p-wave components of the pair potential. Whereas for the helical p-wave junction this phase difference is χ_t for all modes, for the chiral p-wave case the phase difference between singlet and triplet components varies between $\chi_t - \frac{\pi}{2}$ and $\chi_t + \frac{\pi}{2}$. Therefore the results are a weighted average over this range of phase differences. Because the transmission for normal incidence is larger than for oblique incidences there is a difference between $s+$chiral p-wave and $is+$chiral p-wave superconductors, but it is less pronounced than for $(i)s+$helical p-wave superconductors. All pair amplitudes can exist at zero energy for any phase difference between the s-wave and p-wave components of the pair potential.

B. Conductance

The conductance in $s+$chiral p-wave superconductor junctions is different compared to $s+$helical p-wave junctions. First of all, for the $s+$chiral p-wave superconductor there are no sharp peaks at $eV = \Delta_\pm$ because the eigenvalues of the matrix pair potential are complex and angle dependent even for $\chi_t = 0$ [126]. Thus, there is no transition between two sharp peaks and a single broad one when using $(i)s+$chiral p-wave superconductors. Instead, as shown in Fig. 12, the zero-bias conductance is slightly increased by an increase of χ_t, whereas the conductance for $|\Delta_-| < eV < \Delta_+$ is slightly decreased with increasing χ_t.

The difference between the $s+$chiral p- and $is+$chiral p-wave superconductors is most clearly visible around $r = 1$, the transition point between s-wave-dominant and p-wave-dominant superconductors. In contrast with $s+$helical p-wave superconductor junctions, there is no discontinuity in the conductance in either case. For the $s+$chiral p-wave superconductor ($\chi_t = 0$), as shown in Fig. 13(a), the conductance is more similar to the conductance of a junction with an s-wave superconductor, with the zero-bias conductance rapidly increasing as a function of r, and the broad peak around $eV = \Delta_0$ decreasing slowly with r. On the other hand, for the $is+$chiral p-wave superconductor ($\chi_t = 1$), as shown in Fig. 13(b), the conductance is more similar to a p-wave-dominated superconductor. Also for this case, the zero-bias conductance highly depends on r, whereas the peak around $eV = \Delta_0$ develops slowly with decreasing r. Summarizing, for the $(i)s+$chiral p-wave superconductors, the influence of the phase difference χ_t between the s-wave and p-wave components of the pair potential on all properties of the junction is smaller because the phase difference between the singlet and triplet correlations is different for each mode that contributes.

V. 3D B-W SUPERCONDUCTORS

Time-reversal and inversion symmetry broken superconductors are not restricted to two-dimensional materials, but may also appear in three dimensions [84]. Therefore we generalized the formalism to include superconductors whose order parameter depends on $k_{x,y,z}$. For the 3D superconductor, we need to extend the Tanaka-Nazarov boundary conditions. This extension is straightforward. The reflected mode has opposite k_y and k_z instead of only opposite k_y, and integration needs to be performed over a half sphere instead of a half circle. It is assumed that the transmission only depends on the angle made with the surface normal. The inclusion of 3D angles in the

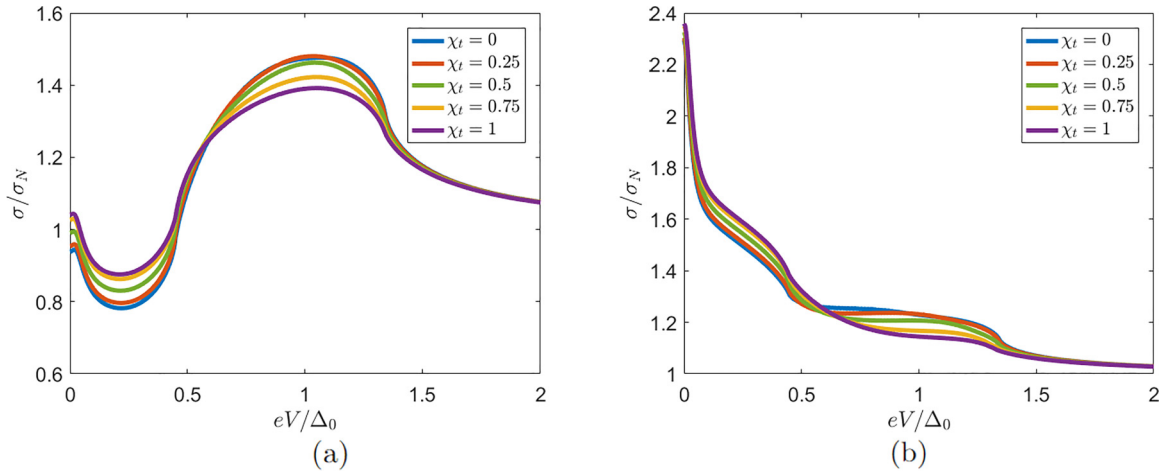

FIG. 12. The dependence of the conductance on χ_t for s-wave-dominant (left, $r = 0.5$) and p-wave-dominant (right, $r = 2$) $(i)s +$ chiral p-wave superconductors. The influence of χ_t on the conductance is comparably small because the phase difference between singlet and triplet pair amplitudes is mode dependent and attains all values. χ_t is determined by this phase difference for the normal mode, which has the largest transmission eigenvalue. Other parameters are set to $\gamma_{\rm BS} = 2$, $z = 0.75$, $E_{\rm Th}/\Delta_0 = 0.02$.

boundary condition does make the code more computationally expensive. However, for certain types of three-dimensional p-wave superconductors symmetry can be exploited to reduce the computational costs.

Specifically, we consider the proximity effect induced by a superconductor with a B-W pair amplitude. The proximity effect of B-W superconductors was first studied for the chargeless helium superfluid [111]. For the B-W phase the d vector is given by $\boldsymbol{d}(\phi, \psi) = (\cos\psi, \sin\psi\sin\phi, \sin\psi\cos\phi)$. The B-W phase is therefore the natural extension of the 2D helical superconductor to a 3D material. The magnitude of the gap is constant over the Fermi surface, and the direction of the d vector is the same as the direction of momentum. Moreover, like the 2D helical superconductor, the 3D B-W superconductor is a topological superconductor protected by time-reversal symmetry [2,125]. The results are therefore predicted to be similar as well.

For the 2D helical superconductors it has been shown following symmetry arguments for the modes at $(k_x, \pm k_y)$ in the absence of a magnetic field only singlet correlations and triplet correlations with d vector proportional to $\langle \boldsymbol{d} \rangle \cdot \boldsymbol{\sigma} = \sigma_x$ are induced [107]. Because in 3D B-W superconductors k_y and k_z are equivalent symmetry dictates that this feature holds for 3D B-W superconductors as well. Even more, this equivalence dictates that the singlet and σ_x-triplet contributions of all modes with fixed k_x are the same. The ϕ-integral can thus be performed analytically and yields a factor 2π. Therefore, for the B-W superconductor we do not need to numerically integrate over two dimensions and the numerical costs are comparable to those for junctions with a 2D superconductor. To improve convergence, a Dynes parameter $\Gamma = 0.01\Delta_0$ was added as an imaginary part of the energy. Here we focus on conductance; the density of states and pair amplitudes are discussed in the Appendix.

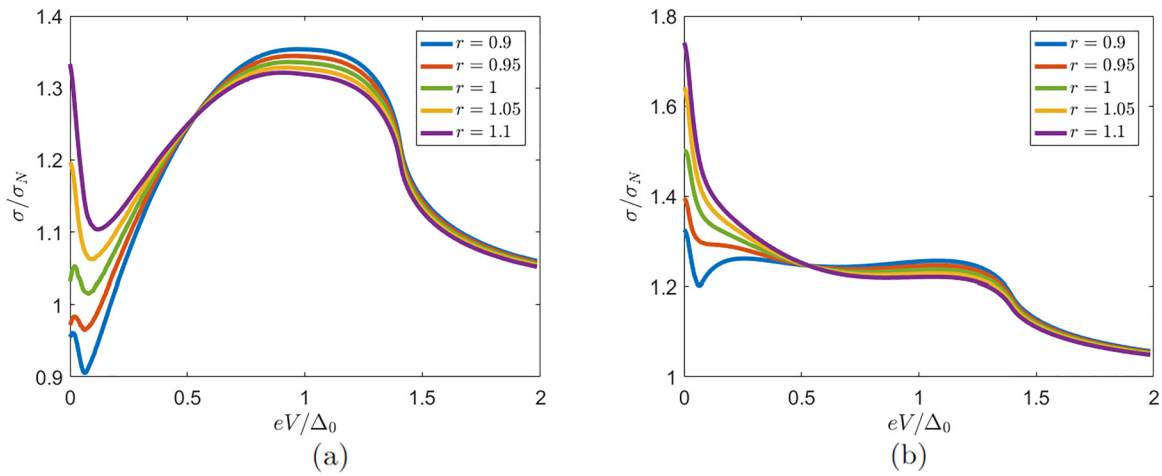

FIG. 13. The transition between the regimes of s-wave-dominant and p-wave-dominant superconductors for the s + chiral p-wave (a) and $is +$ chiral p-wave superconductors (b). For chiral superconductors there is no topological protection even for $\chi_t = 0$, and hence the conductance is always continuous. Other parameters are set to $\gamma_{\rm BS} = 2$, $z = 0.75$, $E_{\rm Th}/\Delta_0 = 0.02$.

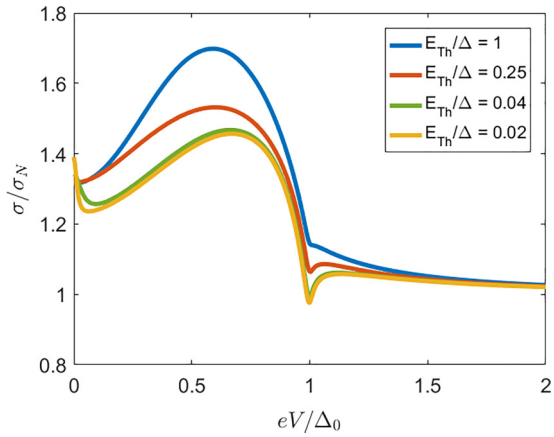

FIG. 14. The conductance in an SNN junction with a B-W-phase p-wave superconductor for different lengths of the junction with $z = 0.75$ and $\gamma_{BS} = 2$. For longer junctions, the peak at zero energy is larger and sharper. For larger voltages σ/σ_N decreases with increasing length.

First, we consider the case of a p-wave B-W superconductor, that is, without inclusion of any s-wave component in the pair potential. The conductance is shown for different lengths in Fig. 14. In long junctions, there is a sharp zero-bias conductance peak with a width on the order of the Thouless energy. For short junctions, however, there exists no zero-bias conductance peak. This is in contrast with other types of p-wave superconductors such as the 2D helical and chiral superconductors described in previous sections.

The absence of a zero-bias conductance peak in the short limit can be understood by considering the tunneling via

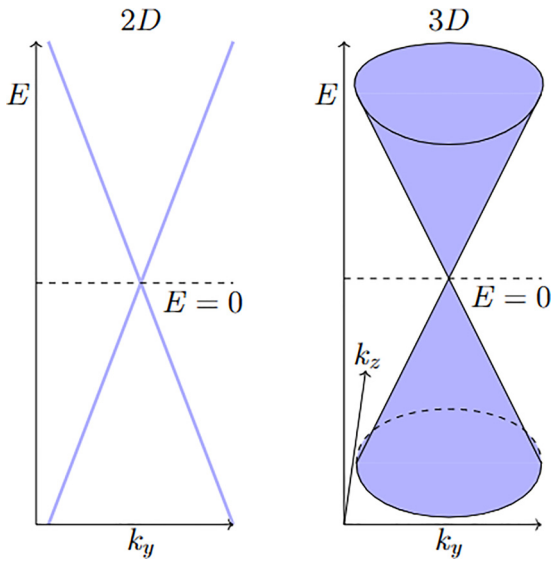

FIG. 15. The dispersion of the Andreev bound states for 2D helical and 3D B-W p-wave superconductors. In both cases, the energy of the bound states is linear in the magnitude of the momentum. For the 2D case, this remains that the density of Andreev bound states is constant around $E = 0$; for the 3D case the density of Andreev bound states vanishes at $E = 0$. Parameters are set to $\gamma_{BS} = 2$, $z = 0.75$, $E_{Th}/\Delta_0 = 0.02$.

Andreev bound states in ballistic junctions, which has a much wider range of possibilities for three-dimensional superconductors compared to their two-dimensional counterparts [109,127–131]. The dispersion of the Andreev bound states in junctions with helical or B-W p-wave superconductors is shown in Fig. 15. In each case there is a zero-energy Andreev state at normal incidence, and the energy is approximately linear in the magnitude of momentum. For 2D superconductors this means that the density of Andreev bound states is approximately constant and finite around $E = 0$ [132,133], leading to a broad conductance peak centered at $eV = 0$. On the other hand, for 3D superconductors, the density of Andreev bound states vanishes at $E = 0$ and is finite for nonzero energies. This leads to an enhancement of the conductance for nonzero voltages compared to the zero-bias conductance. The balance between this effect and coherent Andreev reflection determines whether there is a zero-bias conductance peak or zero-bias conductance dip in junctions with B-W superconductors.

As shown in Fig. 16(a) an increase of the boundary resistance, i.e., an increase γ_{BS}, leads to a suppression of the zero-bias conductance peak but an increase in the conductance peak between $eV = 0.5\Delta_0$ and $eV = \Delta_0$, while the dip around $eV = \Delta_0$ is also more pronounced. The conductance strongly depends on the z parameter, as shown in Fig. 16(b). For small z, that is, an interface with low transparency, the zero-bias conductance consists of the usual sharp peak and an almost flat peak, whereas for large z a zero-bias conductance dip is found. With increasing z also the conductance for $eV \approx \Delta$ is strongly suppressed and may even decrease below the normal-state conductance. These effects can be understood as follows. As γ_{BS} increases the boundary resistance increasingly dominates the total resistance. The coherent Andreev reflection suppresses the resistance inside the bar, but not the boundary resistance. Therefore, the coherent Andreev reflection peak is suppressed if the boundary resistance becomes more dominant. Next, we considered the $s + p$-wave and $is + p$-wave junctions with $E_{Th}/\Delta_0 = 0.02$ and $z = 0.75$. The results in Fig. 17 for $s + p$-wave superconductors are shown and in Fig. 18 for $is + p$-wave superconductors. The main features are similar to that of the two-dimensional helical p-wave superconductors. As shown in Fig. 17(a), if a subdominant B-W pair potential is added to an s-wave superconductor with the same phase, the peak at $eV = \Delta_s$ splits into two peaks at $eV = \Delta_\pm$. The zero-bias conductance is not altered since the B-W superconductor, like the helical superconductor, is a topological superconductor protected by time-reversal symmetry [2,125]. On the other hand, if a subdominant B-W is added to an s-wave superconductor with a phase difference of $\pi/2$, a single peak remains, as highlighted in Fig. 18(a). This peak is suppressed, broadened, and shifted toward slightly lower voltages. The zero-bias conductance is almost constant but slightly increases since in the absence of time-reversal symmetry there is no topological protection.

The case in which the p-wave component of the pair potential is dominant is different compared to the 2D $s +$ helical p-wave superconductors, since the conductance for a 3D p-wave superconductor is different from the conductance for a 2D p-wave superconductor as shown before in Fig. 14. However, the main influence of the inclusion of an s-wave

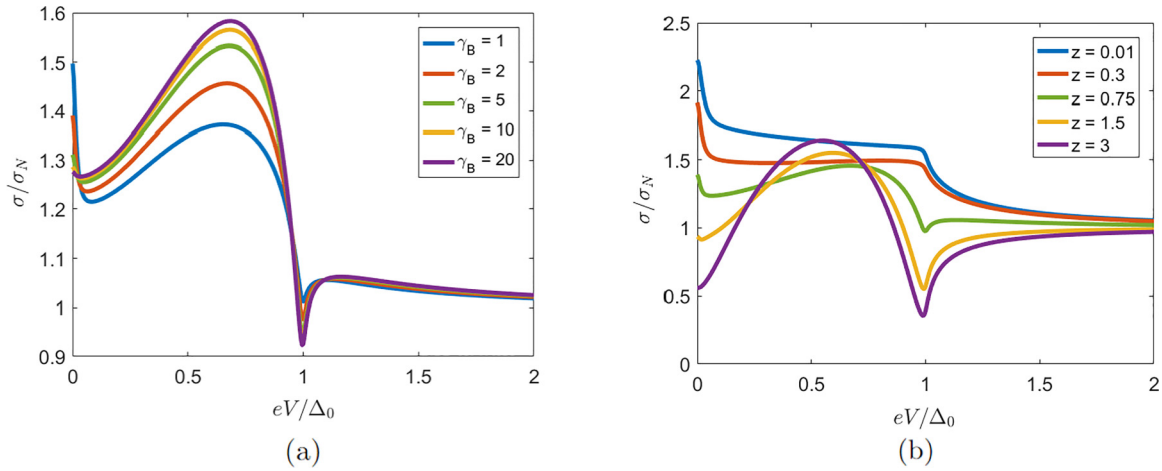

FIG. 16. The dependence of the conductance on the boundary parameters γ_{BS} (left) and z (right) of the s + B-W/N/N junction. The Thouless energy was set to $E_{Th}/\Delta_0 = 0.02$ in all calculations. In the left panel $z = 0.75$; in the right panel $\gamma_{BS} = 2$. An increase of γ_{BS} leads to a decrease of the zero-bias conductance, but an increase of the conductance peak between $eV = 0.5\Delta_0$ and $eV = \Delta_0$. For small z the conductance decreases monotonically with voltage, whereas for large z the peak between $eV = 0.5\Delta_0$ and $eV = \Delta_0$ becomes more pronounced, whereas there exists a zero-bias conductance dip in this case.

component in the pair potential at the same is similar; see Fig. 17(b). The sharp feature in the conductance at $eV = \Delta_p$ splits into two peaks at $eV = \Delta_p \pm \Delta_s$, while the zero-bias conductance is unaltered. For $\Delta_p - \Delta_s \ll \Delta_p$ this peak approaches the zero-bias conductance peak. The two peaks are clearly distinguishable as long as $\Delta_p - \Delta_s \gg E_{Th}$. If time-reversal symmetry is broken, see Fig. 18(b), the zero-bias conductance is decreased if an s-wave component is included in the pair potential, and the peak in the conductance at finite voltage becomes sharper and larger. Moreover, it increases toward $eV = \Delta_0$.

VI. CONCLUSIONS

In conclusion, we have shown that the phase difference that may appear between the singlet and triplet correlations in time-reversal symmetry broken noncentrosymmetric superconductors has a large influence on the local density of states, pair amplitudes, and conductance in dirty SNN junctions. Novel features are particularly visible if the p-wave superconductor is of the 2D helical or 3D B-W type, topological superconductors protected by time-reversal symmetry. We have shown that in the absence of topological protection, the zero-bias conductance varies continuously as a function of the mixing parameter between the s-wave and p-wave components of the pair potential. Our results provide a new way to detect time-reversal symmetry breaking in s + p-wave superconductors. Next to this, they highlight that the breaking of topological protection significantly alters the proximity effect.

For $(i)s +$ chiral p-wave superconductors the phase difference between singlet and triplet components is mode

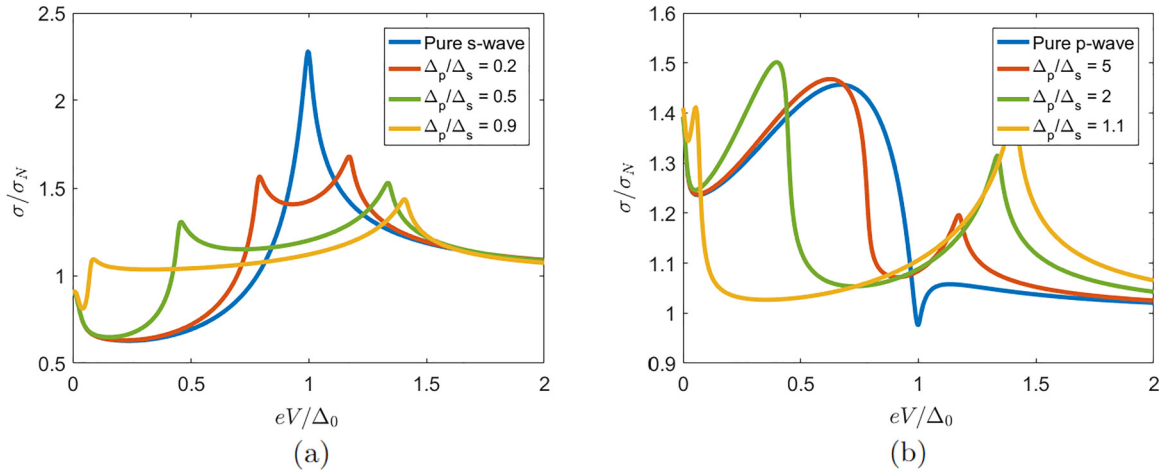

FIG. 17. The conductance of the s+B-W/N/N ($\chi_t = 0$) junction for different ratios of the s-wave and p-wave components of the pair potential. The zero-bias conductance is quantized; it only depends on whether the s-wave or p-wave component of the pair potential is dominant. The height of the zero-bias conductance peak is significantly suppressed compared to the two-dimensional $s +$ helical p-wave junctions. The conductance has sharp features at $eV = E_{Th}$ and $eV = \Delta_\pm$. Parameters are set to $\gamma_{BS} = 2$, $z = 0.75$, $E_{Th}/\Delta_0 = 0.02$.

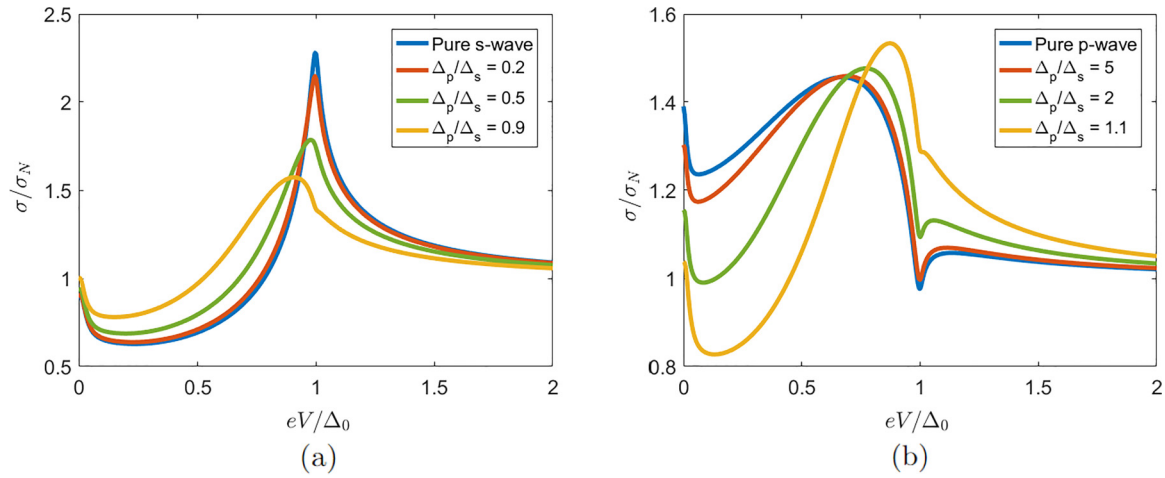

FIG. 18. The conductance of the is+B-W/N/N ($\chi_t = 1$) junction for different ratios of the s-wave and p-wave components of the pair potential. The zero-bias conductance depends on the particular ratio of the s- and p-wave components, crossing the normal-state conductance at $r = 1$. Parameters are set to $\gamma_{\rm BS} = 2$, $z = 0.75$, $E_{\rm Th}/\Delta_0 = 0.02$.

dependent, and therefore the dependence of the density of states and conductance on the phase of the s-wave component of the pair potential is much weaker. Next to this, our results show that a zero-bias conductance peak can be absent when using three-dimensional odd-parity superconductors. This clearly distinguishes three-dimensional odd-parity superconductors from their two-dimensional counterparts.

The main results in our paper depend on the presence of both singlet and triplet correlations, their phase difference, and their relative presence. Our results show that the type of triplet correlations plays an important role as well; the presence or absence of topological invariants crucially influences the dependence on the mixing parameter. Therefore, while several features of our results such as the suppression of the zero-energy (bias) peaks and dips in the density of states (conductance) can be immediately generalized to other inversion and time-reversal symmetry broken superconductors such as $s + (i)f$, $d + (i)p$, and $s +$ helical $p +$ chiral p wave, the behavior around the transition point $r = 1$ can be significantly different for each type of superconductor and needs further investigation.

ACKNOWLEDGMENTS

T.K. and S.B. acknowledge financial support from Spanish MCIN/AEI 10.13039/501100011033 through Projects No. PID2020-114252GB-I00 (SPIRIT) and No. TED2021-130292B-C42, and the Basque Government through Grant No. IT-1591-22. This work was supported by KAKENHI Grants No. 20H00131 and No. 23K17668.

APPENDIX: DENSITY OF STATES AND PAIR AMPLITUDES IN THE $(i)s$+B-W JUNCTION

In this section, we present the density of states and pair amplitudes in junctions with $(i)s$+B-W superconductors.

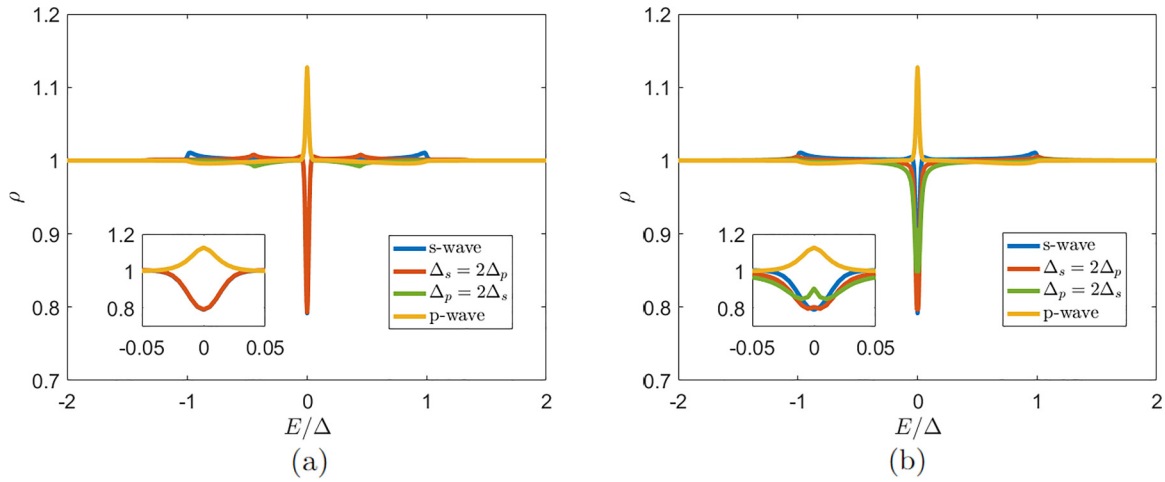

FIG. 19. The local density of states for $s + p$-wave (a) and $is + p$-wave (b) superconductors for s-wave-dominant and p-wave-dominant s+B-W superconductors.

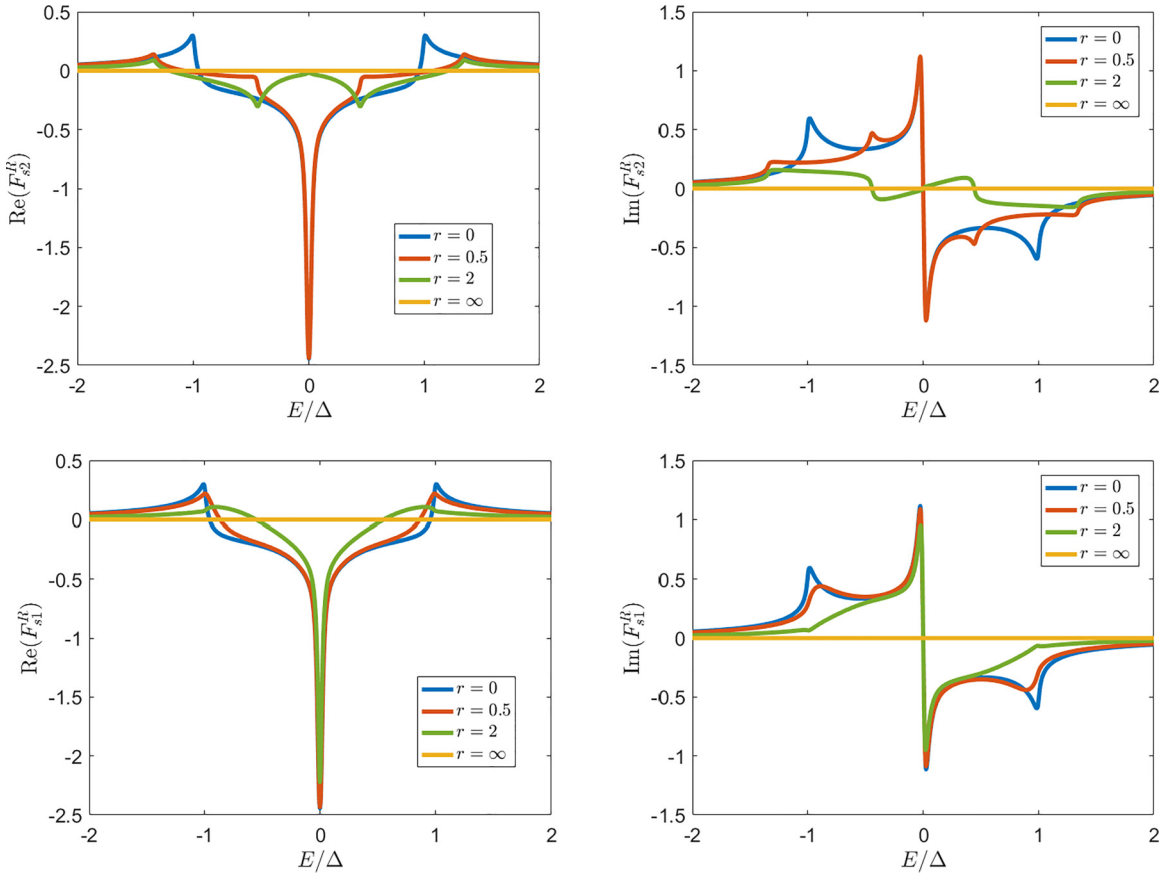

FIG. 20. The singlet pair amplitude for $s + p$-wave (top) and $is + p$-wave (bottom) superconductors for s-wave dominant and p-wave dominant s+B-W superconductors.

We find that the results are similar to those for the two-dimensional junctions with $s +$ helical p-wave superconductors. The density of states and pair amplitudes are shown in Figs. 19–21, respectively. The results are similar to the 2D helical superconductor. For the $s + p$-wave superconductor, the zero-energy density of states is independent of the subdominant component; it depends only on whether the s-wave or p-wave component of the pair potential is dominant. On the other hand, for the $is + p$-wave superconductor, the zero-energy density of states continuously changes from the s-wave to the p-wave value, being lower than the normal density of states for $r = 2$. Because we consider only $s + p$ and $is + p$ wave superconductors the phases of the singlet and triplet components of the pair potential are independent of energy and either only the τ_1 component or only the τ_2 component is nonzero. In the following we show only those pair amplitudes which are not identically zero for all r. The singlet pair amplitude is absent for p-wave superconductors, and has a large peak at $E = 0$ with two smaller peaks at $E = \pm\Delta_0$ for s-wave superconductors. If the s-wave component of the pair potential is dominant the induced singlet pair amplitude peaks at $E = 0$, having exactly (s + $p$wave) or approximately (is +p wave) the same value at zero energy as for the s-wave superconductor.

For s + p-wave superconductors there are peaks at $|E| = \Delta_s \pm \Delta_t$, whereas for is+$p$-wave superconductors there are only broader peaks at $|E| = \Delta_0$. For p-wave-dominant junctions the singlet pair amplitude strongly depends on the relative phase between the s-wave and p-wave components of the pair potential. A common feature it that the singlet pair amplitude is always smaller than in s-wave-dominant junctions. However, for $s + p$-wave superconductors the singlet pair amplitude vanishes at $E = 0$, whereas for $is + p$-wave junctions the singlet pair amplitude has a peak at zero energy. For the triplet pair amplitude the reverse holds. It vanishes for s-wave superconductors, peaks around $E = 0$ for p-wave or p-wave dominant superconductors, and for s-wave dominant superconductors the result highly depends on the phase difference between the s-wave and p-wave components of the pair potential. For s + p-wave superconductors it vanishes at $E = 0$; for $is + p$-wave superconductors the triplet pair amplitude has a peak at zero energy, though it is much smaller than for p-wave (dominant) superconductors.

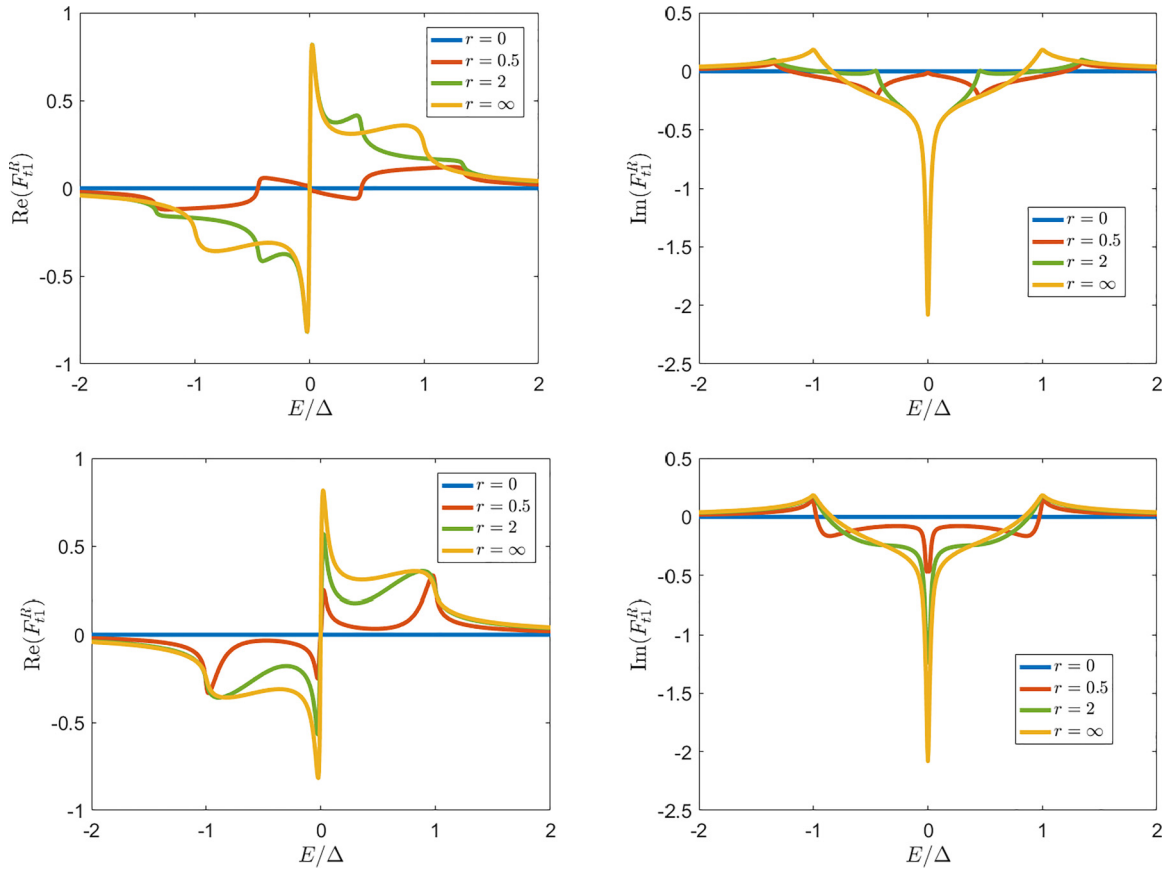

FIG. 21. The triplet pair amplitude for $s + p$-wave (top) and $is + p$-wave (bottom) superconductors for s-wave-dominant and (B-W) p-wave-dominant superconductors.

[1] M. Sigrist and K. Ueda, Rev. Mod. Phys. **63**, 239 (1991).
[2] A. P. Schnyder, S. Ryu, A. Furusaki, and A. W. W. Ludwig, Phys. Rev. B **78**, 195125 (2008).
[3] C. Kallin and A. Berlinsky, J. Phys.: Condens. Matter **21**, 164210 (2009).
[4] Y. Maeno, S. Kittaka, T. Nomura, S. Yonezawa, and K. Ishida, J. Phys. Soc. Jpn. **81**, 011009 (2012).
[5] M. Sigrist, Prog. Theor. Phys. Suppl. **160**, 1 (2005).
[6] A. P. Mackenzie, T. Scaffidi, C. W. Hicks, and Y. Maeno, npj Quantum Mater. **2**, 40 (2017).
[7] C. Kallin and J. Berlinsky, Rep. Prog. Phys. **79**, 054502 (2016).
[8] J. Linder and A. V. Balatsky, Rev. Mod. Phys. **91**, 045005 (2019).
[9] R. Balian and N. Werthamer, Phys. Rev. **131**, 1553 (1963).
[10] L. Fu and C. L. Kane, Phys. Rev. Lett. **100**, 096407 (2008).
[11] S.-P. Chiu, C. Tsuei, S.-S. Yeh, F.-C. Zhang, S. Kirchner, and J.-J. Lin, Sci. Adv. **7**, eabg6569 (2021).
[12] E. Bauer, G. Hilscher, H. Michor, C. Paul, E.-W. Scheidt, A. Gribanov, Y. Seropegin, H. Noël, M. Sigrist, and P. Rogl, Phys. Rev. Lett. **92**, 027003 (2004).
[13] J. Linder and J. W. Robinson, Nat. Phys. **11**, 307 (2015).
[14] H. G. Suh, H. Menke, P. M. R. Brydon, C. Timm, A. Ramires, and D. F. Agterberg, Phys. Rev. Res. **2**, 032023(R) (2020).
[15] D. Aoki, K. Ishida, and J. Flouquet, J. Phys. Soc. Jpn. **88**, 022001 (2019).
[16] S. Saxena, P. Agarwal, K. Ahilan, F. Grosche, R. Haselwimmer, M. Steiner, E. Pugh, I. Walker, S. Julian, P. Monthoux *et al.*, Nature (London) **406**, 587 (2000).
[17] D. Aoki, A. Huxley, E. Ressouche, D. Braithwaite, J. Flouquet, J.-P. Brison, E. Lhotel, and C. Paulsen, Nature (London) **413**, 613 (2001).
[18] F. Hardy and A. D. Huxley, Phys. Rev. Lett. **94**, 247006 (2005).
[19] N. T. Huy, A. Gasparini, D. E. de Nijs, Y. Huang, J. C. P. Klaasse, T. Gortenmulder, A. de Visser, A. Hamann, T. Görlach, and H. v. Löhneysen, Phys. Rev. Lett. **99**, 067006 (2007).
[20] S. Ran, C. Eckberg, Q.-P. Ding, Y. Furukawa, T. Metz, S. R. Saha, I.-L. Liu, M. Zic, H. Kim, J. Paglione *et al.*, Science **365**, 684 (2019).
[21] J. Yang, J. Luo, C. Yi, Y. Shi, Y. Zhou, and G.-q. Zheng, Sci. Adv. **7**, eabl4432 (2021).
[22] Y. Tanaka and S. Kashiwaya, Phys. Rev. B **70**, 012507 (2004).

[23] Y. Tanaka, S. Kashiwaya, and T. Yokoyama, Phys. Rev. B **71**, 094513 (2005).

[24] V. Berezinskii, Pis'ma Zh. Eksp. Teor. Fiz. **20**, 628 (1974) [JETP Lett. **20**, 287 (1974)].

[25] A. Balatsky and E. Abrahams, Phys. Rev. B **45**, 13125 (1992).

[26] D. Belitz and T. R. Kirkpatrick, Phys. Rev. B **46**, 8393 (1992).

[27] E. Abrahams, A. Balatsky, D. J. Scalapino, and J. R. Schrieffer, Phys. Rev. B **52**, 1271 (1995).

[28] T. R. Kirkpatrick and D. Belitz, Phys. Rev. Lett. **66**, 1533 (1991).

[29] P. Coleman, A. Georges, and A. Tsvelik, J. Phys.: Condens. Matter **9**, 345 (1997).

[30] J. Cayao, C. Triola, and A. M. Black-Schaffer, Eur. Phys. J.: Spec. Top. **229**, 545 (2020).

[31] P. Gentile, C. Noce, A. Romano, G. Annunziata, J. Linder, and M. Cuoco, arXiv:1109.4885.

[32] Y. Tanaka and A. A. Golubov, Phys. Rev. Lett. **98**, 037003 (2007).

[33] Y. Tanaka, M. Sato, and N. Nagaosa, J. Phys. Soc. Jpn. **81**, 011013 (2012).

[34] A. Tsintzis, A. M. Black-Schaffer, and J. Cayao, Phys. Rev. B **100**, 115433 (2019).

[35] D. Kuzmanovski, A. M. Black-Schaffer, and J. Cayao, Phys. Rev. B **101**, 094506 (2020).

[36] E. Bauer and M. Sigrist, *Non-Centrosymmetric Superconductors: Introduction and Overview* (Springer Science & Business Media, 2012).

[37] G. Amano, S. Akutagawa, T. Muranaka, Y. Zenitani, and J. Akimitsu, J. Phys. Soc. Jpn. **73**, 530 (2004).

[38] T. Akazawa, H. Hidaka, H. Kotegawa, T. C. Kobayashi, T. Fujiwara, E. Yamamoto, Y. Haga, R. Settai, and Y. Ōnuki, J. Phys. Soc. Jpn. **73**, 3129 (2004).

[39] K. Togano, P. Badica, Y. Nakamori, S. Orimo, H. Takeya, and K. Hirata, Phys. Rev. Lett. **93**, 247004 (2004).

[40] N. Tateiwa, Y. Haga, T. D. Matsuda, S. Ikeda, T. Yasuda, T. Takeuchi, R. Settai, and Y. Ōnuki, J. Phys. Soc. Jpn. **74**, 1903 (2005).

[41] N. Kimura, K. Ito, K. Saitoh, Y. Umeda, H. Aoki, and T. Terashima, Phys. Rev. Lett. **95**, 247004 (2005).

[42] I. Sugitani, Y. Okuda, H. Shishido, T. Yamada, A. Thamizhavel, E. Yamamoto, T. D. Matsuda, Y. Haga, T. Takeuchi, R. Settai *et al.*, J. Phys. Soc. Jpn. **75**, 043703 (2006).

[43] F. Honda, I. Bonalde, K. Shimizu, S. Yoshiuchi, Y. Hirose, T. Nakamura, R. Settai, and Y. Ōnuki, Phys. Rev. B **81**, 140507(R) (2010).

[44] R. Settai, I. Sugitani, Y. Okuda, A. Thamizhavel, M. Nakashima, Y. Ōnuki, and H. Harima, J. Magn. Magn. Mater. **310**, 844 (2007).

[45] E. Bauer, G. Rogl, X.-Q. Chen, R. T. Khan, H. Michor, G. Hilscher, E. Royanian, K. Kumagai, D. Z. Li, Y. Y. Li, R. Podloucky, and P. Rogl, Phys. Rev. B **82**, 064511 (2010).

[46] W. Xie, P. Zhang, B. Shen, W. Jiang, G. Pang, T. Shang, C. Cao, M. Smidman, and H. Yuan, Sci. China Phys. Mech. Astron. **63**, 1 (2020).

[47] K. Ishihara, T. Takenaka, Y. Miao, Y. Mizukami, K. Hashimoto, M. Yamashita, M. Konczykowski, R. Masuki, M. Hirayama, T. Nomoto, R. Arita, O. Pavlosiuk, P. Wiśniewski, D. Kaczorowski, and T. Shibauchi, Phys. Rev. X **11**, 041048 (2021).

[48] F. Wenger and S. Östlund, Phys. Rev. B **47**, 5977 (1993).

[49] D. S. Rokhsar, Phys. Rev. Lett. **70**, 493 (1993).

[50] M. Covington, M. Aprili, E. Paraoanu, L. H. Greene, F. Xu, J. Zhu, and C. A. Mirkin, Phys. Rev. Lett. **79**, 277 (1997).

[51] M. Sigrist, N. Ogawa, and K. Ueda, Physica C **185-189**, 2053 (1991).

[52] R. Laughlin, Physica C **234**, 280 (1994).

[53] R. B. Laughlin, Phys. Rev. Lett. **80**, 5188 (1998).

[54] A. D. Hillier, J. Quintanilla, and R. Cywinski, Phys. Rev. Lett. **102**, 117007 (2009).

[55] R. Wakatsuki, Y. Saito, S. Hoshino, Y. M. Itahashi, T. Ideue, M. Ezawa, Y. Iwasa, and N. Nagaosa, Sci. Adv. **3**, e1602390 (2017).

[56] S. A. Kivelson, A. C. Yuan, B. Ramshaw, and R. Thomale, npj Quantum Mater. **5**, 43 (2020).

[57] J. Xia, Y. Maeno, P. T. Beyersdorf, M. M. Fejer, and A. Kapitulnik, Phys. Rev. Lett. **97**, 167002 (2006).

[58] G. M. Luke, Y. Fudamoto, K. Kojima, M. Larkin, J. Merrin, B. Nachumi, Y. Uemura, Y. Maeno, Z. Mao, Y. Mori *et al.*, Nature (London) **394**, 558 (1998).

[59] J. Clepkens, A. W. Lindquist, and H.-Y. Kee, Phys. Rev. Res. **3**, 013001 (2021).

[60] M. Sigrist, Prog. Theor. Phys. **99**, 899 (1998).

[61] S. K. Ghosh, M. Smidman, T. Shang, J. F. Annett, A. D. Hillier, J. Quintanilla, and H. Yuan, J. Phys.: Condens. Matter **33**, 033001 (2021).

[62] S. K. Ghosh, P. K. Biswas, C. Xu, B. Li, J. Z. Zhao, A. D. Hillier, and X. Xu, Phys. Rev. Res. **4**, L012031 (2022).

[63] W.-C. Lee, S.-C. Zhang, and C. Wu, Phys. Rev. Lett. **102**, 217002 (2009).

[64] C. Farhang, N. Zaki, J. Wang, G. Gu, P. D. Johnson, and J. Xia, Phys. Rev. Lett. **130**, 046702 (2023).

[65] M. Ajeesh, M. Bordelon, C. Girod, S. Mishra, F. Ronning, E. Bauer, B. Maiorov, J. Thompson, P. Rosa, and S. Thomas, arXiv:2305.00589.

[66] T. Shang, M. Smidman, A. Wang, L.-J. Chang, C. Baines, M. K. Lee, Z. Y. Nie, G. M. Pang, W. Xie, W. B. Jiang, M. Shi, M. Medarde, T. Shiroka, and H. Q. Yuan, Phys. Rev. Lett. **124**, 207001 (2020).

[67] V. Grinenko, S. Ghosh, R. Sarkar, J.-C. Orain, A. Nikitin, M. Elender, D. Das, Z. Guguchia, F. Brückner, M. E. Barber *et al.*, Nat. Phys. **17**, 748 (2021).

[68] R. Willa, M. Hecker, R. M. Fernandes, and J. Schmalian, Phys. Rev. B **104**, 024511 (2021).

[69] A. Maisuradze, W. Schnelle, R. Khasanov, R. Gumeniuk, M. Nicklas, H. Rosner, A. Leithe-Jasper, Y. Grin, A. Amato, and P. Thalmeier, Phys. Rev. B **82**, 024524 (2010).

[70] H. S. Røising, G. Wagner, M. Roig, A. T. Rømer, and B. M. Andersen, Phys. Rev. B **106**, 174518 (2022).

[71] R. Movshovich, M. Jaime, M. Hubbard, M. Salamon, A. Balatsky, R. Yoshizaki, and J. Sarrao, J. Phys. Chem. Solids **59**, 2100 (1998).

[72] A. Balatsky, J. Phys. Chem. Solids **59**, 1689 (1998).

[73] V. Belyavsky, V. Kapaev, and Y. V. Kopaev, arXiv:1209.0884.

[74] A. M. Black-Schaffer and C. Honerkamp, J. Phys.: Condens. Matter **26**, 423201 (2014).

[75] Y. Tanaka, Y. Tanuma, and S. Kashiwaya, Phys. Rev. B **64**, 054510 (2001).

[76] M. Sigrist, D. B. Bailey, and R. B. Laughlin, Phys. Rev. Lett. **74**, 3249 (1995).

[77] M. Palumbo, P. Muzikar, and J. A. Sauls, Phys. Rev. B **42**, 2681 (1990).
[78] K. Kuboki and M. Sigrist, J. Phys. Soc. Jpn. **65**, 361 (1996).
[79] Y. Tanuma, Y. Tanaka, M. Ogata, and S. Kashiwaya, Phys. Rev. B **60**, 9817 (1999).
[80] Y. Tanuma, Y. Tanaka, and S. Kashiwaya, Phys. Rev. B **64**, 214519 (2001).
[81] M. Fogelström, D. Rainer, and J. A. Sauls, Phys. Rev. Lett. **79**, 281 (1997).
[82] R. Krupke and G. Deutscher, Phys. Rev. Lett. **83**, 4634 (1999).
[83] M. Matsumoto and H. Shiba, J. Phys. Soc. Jpn. **64**, 4867 (1995).
[84] S. Kanasugi and Y. Yanase, Commun. Phys. **5**, 39 (2022).
[85] T. Kitamura, S. Kanasugi, M. Chazono, and Y. Yanase, Phys. Rev. B **107**, 214513 (2023).
[86] M. Chazono, S. Kanasugi, T. Kitamura, and Y. Yanase, Phys. Rev. B **107**, 214512 (2023).
[87] P. Goswami and B. Roy, Phys. Rev. B **90**, 041301(R) (2014).
[88] D. Möckli and M. Khodas, Phys. Rev. B **99**, 180505(R) (2019).
[89] F. Wilczek, Phys. Rev. Lett. **58**, 1799 (1987).
[90] X.-L. Qi, E. Witten, and S.-C. Zhang, Phys. Rev. B **87**, 134519 (2013).
[91] S. Mishra, Y. Liu, E. D. Bauer, F. Ronning, and S. M. Thomas, Phys. Rev. B **106**, L140502 (2022).
[92] Z. Wu, Y. Fang, H. Su, W. Xie, P. Li, Y. Wu, Y. Huang, D. Shen, B. Thiagarajan, J. Adell, C. Cao, H. Yuan, F. Steglich, and Y. Liu, Phys. Rev. Lett. **127**, 067002 (2021).
[93] C. Iniotakis, N. Hayashi, Y. Sawa, T. Yokoyama, U. May, Y. Tanaka, and M. Sigrist, Phys. Rev. B **76**, 012501 (2007).
[94] M. Eschrig, C. Iniotakis, and Y. Tanaka, Properties of interfaces and surfaces in non-centrosymmetric superconductors, in *Non-Centrosymmetric Superconductors: Introduction and Overview*, edited by E. Bauer and M. Sigrist (Springer, Berlin, 2012), pp. 313–357.
[95] G. Annunziata, D. Manske, and J. Linder, Phys. Rev. B **86**, 174514 (2012).
[96] Y. Rahnavard, D. Manske, and G. Annunziata, Phys. Rev. B **89**, 214501 (2014).
[97] V. Mishra, Y. Li, F.-C. Zhang, and S. Kirchner, Phys. Rev. B **103**, 184505 (2021).
[98] S. Ikegaya, S.-I. Suzuki, Y. Tanaka, and D. Manske, Phys. Rev. Res. **3**, L032062 (2021).
[99] A. Daido and Y. Yanase, Phys. Rev. B **95**, 134507 (2017).
[100] S.-P. Chiu, V. Mishra, Y. Li, F.-C. Zhang, S. Kirchner, and J.-J. Lin, Nanoscale **15**, 9179 (2023).
[101] Y. Asano and S. Yamano, Phys. Rev. B **84**, 064526 (2011).
[102] L. Klam, A. Epp, W. Chen, M. Sigrist, and D. Manske, Phys. Rev. B **89**, 174505 (2014).
[103] S. Wu and K. V. Samokhin, Phys. Rev. B **80**, 014516 (2009).
[104] S. Fujimoto, Phys. Rev. B **79**, 220506(R) (2009).
[105] K. Børkje and A. Sudbø, Phys. Rev. B **74**, 054506 (2006).
[106] Y. Tanaka, T. Kokkeler, and A. Golubov, Phys. Rev. B **105**, 214512 (2022).
[107] T. H. Kokkeler, Y. Tanaka, and A. A. Golubov, Phys. Rev. Res. **5**, L012022 (2023).
[108] T. Kokkeler, A. Hijano, and F. S. Bergeret, Phys. Rev. B **107**, 104506 (2023).
[109] L. J. Buchholtz and G. Zwicknagl, Phys. Rev. B **23**, 5788 (1981).
[110] L. J. Buchholtz, Phys. Rev. B **33**, 1579 (1986).
[111] S. Higashitani, Y. Nagato, and K. Nagai, J. Low Temp. Phys. **155**, 83 (2009).
[112] W. Belzig, F. K. Wilhelm, C. Bruder, G. Schön, and A. D. Zaikin, Superlattices Microstruct. **25**, 1251 (1999).
[113] V. Chandrasekhar, Proximity-coupled systems: Quasiclassical theory of superconductivity, in *Superconductivity: Conventional and Unconventional Superconductors*, edited by K. H. Bennemann and J. B. Ketterson (Springer, Berlin, 2008), pp. 279–313.
[114] R. Dingle, Proc. R. Soc. London A **201**, 545 (1950).
[115] V. Gantmakher, *Electrons and Disorder in Solids* (Oxford University Press, 2005).
[116] Y. Tanaka, Y. V. Nazarov, and S. Kashiwaya, Phys. Rev. Lett. **90**, 167003 (2003).
[117] Y. Tanaka, Y. V. Nazarov, A. A. Golubov, and S. Kashiwaya, Phys. Rev. B **69**, 144519 (2004).
[118] Y. V. Nazarov, Superlattices Microstruct. **25**, 1221 (1999).
[119] A. Schmid and G. Schön, J. Low Temp. Phys. **20**, 207 (1975).
[120] T. T. Heikkilä, M. Silaev, P. Virtanen, and F. S. Bergeret, Prog. Surf. Sci. **94**, 100540 (2019).
[121] M. Sato and Y. Ando, Rep. Prog. Phys. **80**, 076501 (2017).
[122] M. Leijnse and K. Flensberg, Semicond. Sci. Technol. **27**, 124003 (2012).
[123] C.-K. Lu and S. Yip, Phys. Rev. B **78**, 132502 (2008).
[124] S. Ikegaya, S.-I. Suzuki, Y. Tanaka, and Y. Asano, Phys. Rev. B **94**, 054512 (2016).
[125] Y. Tanaka, T. Yokoyama, A. V. Balatsky, and N. Nagaosa, Phys. Rev. B **79**, 060505(R) (2009).
[126] P. Burset, F. Keidel, Y. Tanaka, N. Nagaosa, and B. Trauzettel, Phys. Rev. B **90**, 085438 (2014).
[127] Y. Asano, Y. Tanaka, Y. Matsuda, and S. Kashiwaya, Phys. Rev. B **68**, 184506 (2003).
[128] T. Löfwander, V. Shumeiko, and G. Wendin, Supercond. Sci. Technol. **14**, R53 (2001).
[129] A. Yamakage, K. Yada, M. Sato, and Y. Tanaka, Phys. Rev. B **85**, 180509(R) (2012).
[130] S. Tamura, S. Kobayashi, L. Bo, and Y. Tanaka, Phys. Rev. B **95**, 104511 (2017).
[131] L. Fu and E. Berg, Phys. Rev. Lett. **105**, 097001 (2010).
[132] M. Matsumoto and M. Sigrist, J. Phys. Soc. Jpn. **68**, 994 (1999).
[133] A. Furusaki, M. Matsumoto, and M. Sigrist, Phys. Rev. B **64**, 054514 (2001).